Progress in Nuclear Energy 153 (2022) 104404

Contents lists available at ScienceDirect

Progress in Nuclear Energy

journal homepage: www.elsevier.com/locate/pnucene

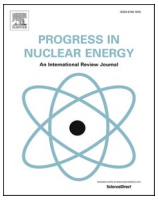

Review

Review of instabilities produced by direct contact condensation of steam injected in water pools and tanks

J.L. Muñoz-Cobo *, D. Blanco, C. Berna, Y. Córdova

Universitat Politècnica de València, Instituto de Ingeniería Energética, Camino de Vera s/n 46022, Valencia, Spain

ARTICLE INFO

Keywords:
Chugging
Condensation oscillations
Direct contact condensation
Bubbling condensation oscillations
Steam discharge instabilities

ABSTRACT

The purpose of this paper is to review and analyze several types of instabilities as condensation oscillations (CO), stable condensation oscillations (SC), and bubbling condensation oscillation (BCO). These instabilities are produced during the discharge of steam into subcooled pools through vents or spargers. The mechanism of direct contact condensation (DCC) plays an essential role in these instabilities justifying that we review first the fundamental basis of DCC and the jet penetration length for the discharges of pure steam in subcooled water. Then, special attention is devoted to developing correlations for the nondimensional penetration length for ellipsoidal or hemi-ellipsoidal prolate steam jets observed in many experiments, to the heat transfer coefficients of DCC and to the best way to correlate the penetration length. Next, it is analyzed the stability of the steam jets with hemi-ellipsoidal shape in the transition and condensation oscillation regimes and it is computed the subcooling temperature threshold for low and high oscillation frequencies. These results for the subcooling temperature thresholds for low and high frequencies with a hemi-ellipsoidal steam jet are then compared with the results for spherical and cylindrical jets and with the experimental data in an interval of mass fluxes ranging from 0 to 180 kg/m^2s. In addition, a sensitivity analysis is performed to know the dependence of the low and high frequency liquid temperature thresholds on the vent diameter and the polytropic coefficient. The third part of the paper is devoted to the study of the instabilities produced in the stable condensation (SC) and the interfacial condensation oscillations (IOC) regions of the map. First Hong et al. model (2012) is extended to include the entrainment in the liquid dominated region (LDR), obtaining new expressions for the oscillations frequency that depend on the entrainment coefficient and the expansion of the jet in the liquid dominated region. Finally, the mechanical energy balance is extended to include the momentum transferred to the jet by the condensate steam, obtaining a new equation for the frequency that is compared with Hong et al.'s data for a set of pool temperatures ranging from 35 °C to 90 °C and discharge mass steam fluxes ranging from 200 to 900 kg/m^2s.

1. Introduction

Discharges of pure steam or its mixtures with non-condensable gases into subcooled water pools and water tanks through nozzles, vents, blowdown pipes, injectors or spargers is an issue of interest in the nuclear energy field. Since this industry widely uses these discharges in practically all types of nuclear power plants and in different kinds of applications (Cumo et al., 1977; Zhao et al., 2016 and 2020, De With 2009, Song and Kim 2011, Hong et al., 2012, Villanueva et al., 2015, Wang et al., 2021). In these discharges of steam or gas mixtures, there is a significant exchange of mass and energy at the interface between the gas and liquid phases through the mechanism known as direct contact condensation (DCC). In addition, DCC is also an issue of interest in the design of industrial equipment such as contact feedwater heaters, contact condensers and cooling towers (Sideman and Moalem-Maron 1982). The correct prediction of the condensing mass flow rate and the heat rate exchanged at the interface with and without NC gases is an essential factor to know the pool heating rate and the gas mass flow rate that reaches the free surface of the pool (Song and Kim 2011). Since this steam increases the pressure in the gas phase, this subject is also of interest in the containment design of nuclear power plants. Another issue of importance for these discharges is that these local discharges can produce mainly five types of instabilities known as "chugging" (C), "condensation oscillations" (CO), "bubbling condensation oscillations" (BCO), stable condensation oscillations (SC), and "interfacial oscillation condensation" (IOC), depending on the boundary conditions of the

* Corresponding author.
E-mail addresses: jlcobos@iqn.upv.es (J.L. Muñoz-Cobo), dablade@upv.es (D. Blanco), ceberes@iie.upv.es (C. Berna), yaiselcc92@gmail.com (Y. Córdova).

https://doi.org/10.1016/j.pnucene.2022.104404
Received 24 March 2022; Received in revised form 18 July 2022; Accepted 29 August 2022
Available online 19 September 2022

injection, which are described with detail below in this section. The study of these thermal-hydraulic instabilities is important from the safety point of view because of can produce undesirable pressure spikes on the containment and thermal stratification in the suppression pool (Gregu et al., 2017). In addition, the mechanism known as condensation induced water-hammer (CIWH) can appear when a large bubble or pocked of steam is surrounded by subcooled water with a sizeable interfacial contact area; in these conditions, the steam pocket can collapse, inducing pressure oscillations (Urban and Schlüter 2014).

Another aspect to be considered, as mentioned by Villanueva et al. (2015), is that the steam discharged through the spargers in a subcooled pool, which is used as a sink for the heat released during an accidental event, is a source of mass (steam or steam + NC), energy and momentum for the pool. The energy released through the spargers is exchanged through the interface with the pool liquid phase. In addition, the steam mass flow rate can condense totally or partially at the jet-liquid interface, releasing the phase-change heat, which increases the pool temperature locally. This local increment of the pool temperature could cause thermal stratification if the fluid located near the jet interface does not mix properly with the rest of the subcooled water of the pool (Li et al., 2014). The amount of momentum transported by the gas discharged in the pool can produce, by the shear stress exerted by the gas fluid on the liquid at the interface and by the momentum transfer during the condensation process, an increase of the liquid velocity surrounding the jet interface that facilitates the thermal mixing in the pool. In addition, if the momentum transported by the gas phase is big enough, this momentum transfer could induce instabilities of Kelvin-Helmholtz type at the jet interface, as has been recently studied by Sun et al. (2020). But at low steam mass flow rates without non-condensable gases and assuming that the pool is subcooled, the high condensation rates at the interface will produce an oscillating behavior known as condensation oscillation. These oscillations for pure steam can be of several types depending on the steam mass flux G_0 at the pipe exit and the temperature difference $\Delta T = T_s - T_l$, between the steam and the subcooled water (Song and Kim 2011; Li et al., 2014). When non-condensable gases are present, the condensation of the steam at the interface produces an accumulation of non-condensable gases near the interface that diminish the direct contact condensation of the steam and degrades the condensation heat transfer coefficients, so the regime map changes depending on the mass fraction of NC in the gas mixture. For pure steam, the condensation regime map in terms of pool temperature and mass flux has been obtained by several authors as Chan and Lee (1982) as displayed in Fig. 1, Cho et al. (1998) by visual observations and acoustic methods as shown in Fig. 2 and by Aya and Nariai (1991). Also, notice that the lines of Fig. 1 separating the different condensation regimes can change with the sparger or nozzle diameter. However, these changes are not very pronounced, as observed by Song and Kim (2011).

In general, these maps contain six regions: the chugging region

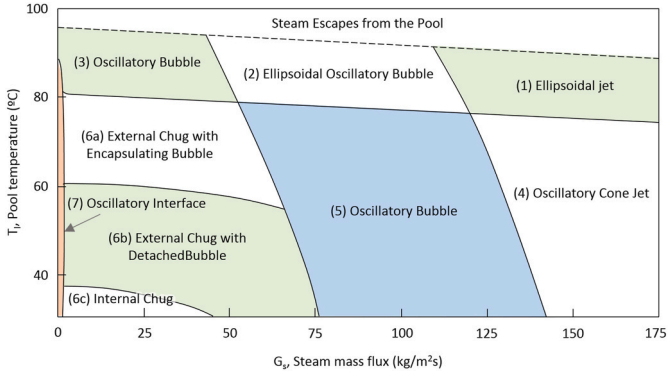

Fig. 1. Regime map for direct contact condensation obtained by Chan and Lee (1982).

denoted by (C), which occurs at relatively low steam mass flux and high subcooling. In this region, steam bubbles are formed outside the injection pipe and collapse periodically, and therefore, the water from the pool flows back entering the pipe exit region. Then, the pressure increases in the pipe, and the steam exits again and forms bubbles that collapse and the previous process is repeated. In the condensation oscillations region (CO), the interface oscillates violently, the steam condenses outside the nozzle, and the surrounding water moves back and for following these oscillations. The TCO is the region of transition from chugging to condensation oscillations, with the characteristic that the subcooled water does not enter the nozzle. The SC region, which occurs for higher steam mass flux and high subcooling, is the region where stable condensation happens and only the jet end oscillates importantly. There are two additional regions when the pool temperature rises above 80 °C and is approximately below 92 °C. The first one, below a mass flux of 340 kg/m^{2}s, is the BCO or bubbling condensation oscillation region, where irregular bubbles detach from the discharge pipe, and then condense or escape. The second one, above this max flux value, is the IOC or interfacial oscillation condensation region characterized by the non-stable character of the jet interface (Hong et al., 2012).

Norman et al. (2006) performed a detailed analysis and a set of experiments on jet-plume condensation of steam-air mixture discharges in a subcooled water pool. The objective was to study all the phenomena that appear in the three regions of a buoyant gas jet: the momentum dominated region, the transition region and the ascending plume dominated by buoyancy forces, and in addition, the thermal response of the pool. Norman et al. performed the study for different vent sizes, different mass flow rates, different degrees of subcooling in the pool, and finally, different mass fractions of non-condensable gases in the mixture. Then Norman and Revankar (2010-a) and Norman and Revankar (2010-b) completed this work with two papers on this same issue.

The discharges of mixtures of steam and NC gases as air has been performed more recently by several authors as Qu and Tian (2016), which have conducted experiments on condensation of a steam–NC mixture jet discharged in the bottom of a subcooled water tank. They observed that the momentum-dominated region becomes an ascending plume formed by tiny bubbles after losing its initial momentum.

This paper's main goal is to study and deeply analyze the jet condensation-oscillations produced by the discharges of a steam flow into a subcooled pool. First, it has been reviewed the works of Fukuda (1982) , Fukuda and Saitoh (1982) and Aya et al. (1980, 1986, 1991), extending these studies to ellipsoidal condensing-jet shapes, considering recent advances performed by authors as Villanueva et al. (2015), and Gallego-Marcos et al. (2019) for the estimation of the average heat transfer coefficient (HTC). Then, we study the capability of Fukuda and Saitoh. models extended to hemi-spherical prolate steam jets to predict the subcooling threshold for the transition and condensation oscillation regimes when incorporating Gallego-Marcos et al. correlation for the HTC. In addition, it is performed a comparison of these model predictions with the experimental data for low and high frequency pressure oscillations. Furthermore, this paper also studies the instabilities produced in the SC and IOC regimes, calculating the frequency predictions with different models, and comparing the results with Hong et al.'s (2012) experimental data.

The organization of the paper is as follows: first, in section 2 we have reviewed, the direct contact condensation heat transfer and the penetration length of a steam jet discharged into a subcooled pool. Then we have used these analyses as support for section 3. In sections 3.1, 3.2, and 3.3 we have performed a revision of the oscillations of discharged steam jets into subcooled water pools in the following map regions: transition condensation (TCO), condensation oscillation (CO), and bubbling condensation oscillation (BCO). Then, in section (3.4) we have conducted the study of the oscillations in the stable condensation (SC) and the interfacial oscillation condensation (IOC) map regions. Finally, in section 4, we have discussed the main conclusions and new research areas of interest in this field.

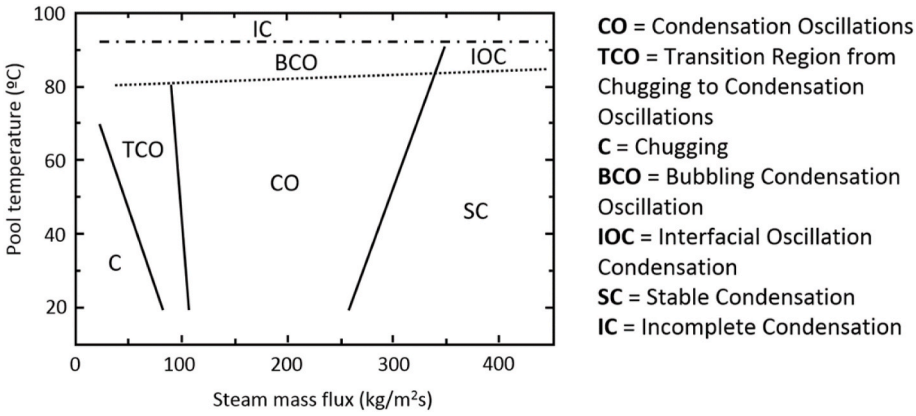

Fig. 2. Condensation regime map for direct contact condensation (DCC) according to Cho et al. (1998).

2. Fundamentals of direct contact condensation heat transfer and jet penetration length

2.1. Direct contact condensation heat transfer

The first theories on direct contact condensation were based on kinetic theory, Schrage (1953) conducted a theoretical study on the interphase heat transfer and deduced, based on kinetic theory, expressions for the net mass flux m_i'' and the net heat flux q_i''condensing at the interface and which are given by:

$$q_i'' = h_{fg}\, m_i'' = h_{fg}\left(\frac{M}{2\pi R}\right)^{1/2}\left(\widehat{f}_c\frac{\Gamma(a)p_v}{T_v^{1/2}} - \widehat{f}_e\frac{p_l}{T_l^{1/2}}\right) \tag{1}$$

Where $\widehat{f}_c$ is known as the accommodation coefficient for condensation while, $\widehat{f}_e$ is the accommodation coefficient for evaporation, M is the molecular weight of the steam, R is the gas constant. In addition, p_v is the vapor pressure, T_v is the vapor temperature, p_l is the liquid pressure and T_l the liquid temperature, and h_{fg} is the specific enthalpy of phase change. The standard value of $\frac{R}{M} = 462\,\frac{J}{kg^oK}$ for pure steam is used, and finally, $\Gamma(a)$ is given by the expression:

$$\Gamma(a) = \exp\left(a^2\right) + a\sqrt{\pi}(1+\mathrm{erf}(a)) \tag{2}$$

Being $\mathrm{erf}(a)$ the mathematical error function. The physical meaning of $\Gamma(a)$ is that this coefficient, according to Collier (1981), results from the net motion of the steam toward the interface and this motion is superimposed on the motion produced by the Maxwell distribution. The expression for a is given by the ratio of the steam velocity component w, normal to the interface that is produced by the steam condensation and the characteristic molecular steam velocity in kinetic theory:

$$a = \frac{w}{\sqrt{\frac{2RT}{M}}} = \frac{q_i''}{h_{fg}\varrho_v\sqrt{\frac{2RT}{M}}} \tag{3}$$

For high-temperature condensing processes like the one for water steam, the value of a is normally small; for instance, for a heat condensing flow of $100\,kw/m^2$, the value of a is $1.3\,10^{-4}$, but when the condensation mass flux increases, then the value of a also increases. For small values of a, $\Gamma(a)$ can be approximated by the expression (Carey 1992):

$$\Gamma(a) \approx 1 + \sqrt{\pi}a = 1 + \sqrt{\pi}\,\frac{q_i''}{h_{fg}\varrho_v\sqrt{\frac{2RT}{M}}} \tag{4}$$

Substituting the value of $\Gamma(a)$ given by expression (4), in equation (1), and clearing q_i'', yields the expression obtained by Silver and Simpson (1961) and if the accommodation coefficients for evaporation and condensation have the same value:

$$q_i'' = \left[\frac{2\widehat{f}}{2-\widehat{f}}\right]h_{fg}\left(\frac{M}{2\pi R}\right)^{1/2}\left(\frac{p_v}{T_v^{1/2}} - \frac{p_l}{T_l^{1/2}}\right) \tag{5}$$

Several efforts have been conducted to obtain the accommodation coefficient. Marek and Straub (2001) performed a fitting to the data of Finkelstein and Tamir (1976) and obtained the following expression for $\widehat{f}$, which diminish when the pressure increases:

$$\widehat{f}\,(p) = 5.9083\;10^{-3}\left(\frac{p}{p_0}\right)^{-1.3686} \tag{6}$$

Being p_0 a reference pressure that is taken equal to 1 bar, this effect is a consequence of considering the gas as a real gas. In addition, Komnos (1981) considers the deviation in the gas behavior from that of an ideal gas and obtained for the accommodation coefficient the following correlation based on the specific volume of the steam:

$$\widehat{f}\,(p) = 0.05\,\frac{v_v(p)}{v_v(p_0)} \tag{7}$$

Another common formula to express equation (5) is to consider $p_v = \rho_v\left(\frac{R}{M}\right)T_v$, $p_l = \rho_v^{sat}(T_l)\left(\frac{R}{M}\right)T_l$, and $\frac{R}{M} = \frac{k_B}{m}$, being k_B the Boltzmann constant and m the mass of a molecule of steam. In this case, equation (5) is also usually expressed in the form:

$$q_i'' = \left[\frac{2\widehat{f}}{2-\widehat{f}}\right]h_{fg}\left(\frac{k_B}{2\pi m}\right)^{1/2}\left(\rho_v T_v^{1/2} - \rho_{sat}^v(T_l)T_l^{1/2}\right) \tag{8}$$

Chandra and Keblinski (2020) used molecular dynamics to obtain the accommodation coefficient $\widehat{f}$. They obtained that the accommodation coefficients depend on the liquid temperature near the interface, and they provide the following law that fit well their results and the previously calculated ones by other authors:

$$\widehat{f}\,(T_l) = -4.16\;10^{-6}(T_l)^2 + 2.15\;10^{-3}T_l + 0.73 \tag{9}$$

Also, Labuntsov, and Muratova and Labuntsov (Kryukov et al., 2013) have solved the Boltzmann kinetic equation for weak evaporation and condensation, deducing more accurate formulas than equation (5) for non-equilibrium condensation and evaporation processes, in this case, they found:

$$q_i'' = \left[\frac{2\widehat{f}}{2-0.798\,\widehat{f}}\right]h_{fg}\left(\frac{k_B}{2\pi m}\right)^{1/2}\left(\rho_v T_v^{1/2} - \rho_{sat}^v(T_l)T_l^{1/2}\right) \tag{10}$$

Expression (10) is helpful to obtain upper limits for the direct contact condensation heat flux.

2.2. Jet penetration length for discharges of pure steam

One of the first semi-empirical derivations of the jet penetration length for a steam-jet discharging in a subcooled water pool was obtained by Kerney et al. (1972). First, these authors deduced a semi-empirical formula for the penetration length and then they improved this expression by fitting the coefficients and exponents to the experimental data. Denoting by h the local heat transfer coefficient from the steam to the water, by $W_s(x) = \pi r^2 G(x)$ the steam mass flow rate at the axial position x, and by $m_c''(x)$, the condensation mass flux at the interface, then the change of the steam mass flow rate along x is given by the equation:

$$\frac{d}{dx}W(x) = -2\pi r m_c''(x) \quad with m_c''(x)h_{fg} = h(T_s - T_\infty) \tag{11}$$

Equation (11) can be written after some calculus because of the expressions for $m_c''(x)$ and $W(x)$ and after dividing by the mass flow rate W_0 at the nozzle exit in the form:

$$\frac{d}{dx^+}\left(\frac{W_s(x^+)}{W_{s,0}}\right)^{1/2} = -\left(\frac{G}{G_0}\right)^{\frac{1}{2}} S_m\, B \tag{12}$$

Where $x^+ = x/r_0$, is the dimensionless axial distance, B is the condensation driving potential defined by the expression

$$B = \frac{c_p(T_s - T_\infty)}{h_{fg}} \tag{13}$$

Being T_s the saturation temperature and T_∞ the bulk temperature of the pool. Finally, S_m is a nondimensional number analogous to the Stanton number, and defined for this case as follows:

$$S_m = \frac{h}{c_p G} \tag{14}$$

Equation (12) can be integrated with the boundary conditions at the nozzle exit and at the penetration length $l_p$of the jet where all the steam is condensed, so it is obtained:

$$\frac{W_s}{W_{s,0}} = 1 \text{ at } x^+ = 0, \text{ and } \frac{W_s}{W_{s,0}} = 0 \text{ at } x^+ = \frac{l_p}{r_0} \tag{15}$$

To integrate equation (12), it is necessary to know how $G(x^+)$ changes with x^+, and S_m with x^+. Assuming some average values G_m for G and $\overline{S}_m$ for S_m, the integration of (12) yields for the dimensionless steam penetration length $X_p$the following result deduced by Kerney et al. (1972):

$$X_p = \frac{2l_p}{D_0} = \overline{S}_m^{-1} B^{-1}\left(\frac{G_0}{G_m}\right)^{1/2} \tag{16}$$

Kerney et al. chose for G_m the value of 275 kg/m^{2}s because the data of their experiments were obtained with choked injector flows and the remaining effects were included in the transport modulus $\overline{S}_m$, which is obtained experimentally. The 128 experiments performed by these authors cover an extensive range of boundary conditions, the injector diameters D_0 were in the range $0.0004 - 0.0095\ m$, the mass fluxes G of the experiments were in the range $332 - 2044 \frac{kg}{m^2 s}$, the bulk temperature of the pool denoted by T_∞ was in the range $301 - 352\ K$ at atmospheric pressure, the condensation driving potential B was in the range $0.0473 - 0.1342$. Then, Kerney et al. performed a fit to their data in terms of B and $\left(\frac{G_0}{G_m}\right)$, obtaining that the expression that best fit the data was:

$$X_p = \frac{2l_p}{D_0} = 0.7166\, B^{-0.8411}\left(\frac{G_0}{G_m}\right)^{0.6466} \tag{17}$$

Also, these authors give an expression based on equation (16), using the assumption of Linehan and Grolmes (1970) that a constant transport modulus $\overline{S}_m$, provides a reasonable correlation and includes all the remaining effects in the value of the transport modulus.

Petrovic (2005), after performing a parametric study of the shape of the steam plumes for different boundary conditions, arrived at the conclusion that for conditions of high steam mass flux, high pool temperature and small diameter of the injectors the shape of the steam plume is ellipsoidal. Assuming an axisymmetric plume of length l_p, as displayed in Fig. 3a, the variation of the plume radius $r(x)$ with the distance is:

$$r(x) = r_0\sqrt{1 - \frac{x^2}{l_p^2}} \tag{18}$$

Because of the element of the interfacial area $dS = 2\pi r(x)\sqrt{1 + (r'(x))^2}\, dx$for direct contact condensation changes with the distance, then the expression for the mass flow rate change is given instead of equation (11) by:

$$dW_s(x) = -2\pi r(x)\sqrt{1 + (r'(x))^2}\, m_c''\, dx = -2\pi r(x)\sqrt{1 + (r'(x))^2}\, \frac{h(T_s - T_\infty)}{h_{fg}}\, dx \tag{19}$$

Integrating expression (19) between $x = 0, W_s(0) = W_{s,0}$, and $x = l_p$, with $W_s(l_p) = 0$ yields for the case of an ellipsoidal steam plume:

$$W_{s,0} = \frac{\overline{h}\Delta T}{h_{fg}} A_i = \frac{\overline{h}\Delta T}{h_{fg}} 2\pi \int_0^{l_p} r(x)\sqrt{1 + (r'(x))^2}\, dx \tag{20}$$

Being A_i the interfacial area between the steam and liquid phases, $\overline{h}$ the average heat transfer coefficient.

After some calculus it is obtained assuming that $r(x)$ is given by equation (18) the following result:

$$W_{s,0} = \frac{\overline{h}\Delta T}{h_{fg}} \frac{\pi r_0 l_p}{\left(1 - \frac{r_0^2}{l_p^2}\right)^{1/2}} \left\{ arcsin\left(1 - \frac{r_0^2}{l_p^2}\right)^{1/2} + \frac{r_0}{l_p}\left(1 - \frac{r_0^2}{l_p^2}\right)^{1/2} \right\} \tag{21}$$

If the injector exit radius $r_0$is much smaller than the steam penetration length l_p, i.e., $r_0 \ll l_p$, then equation (21) can be approximated retaining only first-order terms in $\frac{r_0}{l_p}$:

$$W_{s,0} = \frac{\overline{h}\Delta T}{h_{fg}} \pi r_0 l_p \left\{ \frac{\pi}{2} + \frac{r_0}{l_p} \right\} \tag{22}$$

Consequently, when $r_0 \ll l_p$ the interfacial area can be approximated up to first order by:

$$A_i = \pi r_0 l_p \left\{ \frac{\pi}{2} + \frac{r_0}{l_p} \right\} \tag{23}$$

from equation (22), it is deduced the following expression for the dimensionless penetration length:

$$X_p = \frac{l_p}{r_0} = \frac{2l_p}{D_0} = \frac{2}{\pi}\left(\frac{G_0 h_{fg}}{\overline{h}\Delta T} - 1\right) = 0.6366\left\{ B^{-1}\overline{S}_m^{-1}\left(\frac{G_0}{G_m}\right) - 1 \right\} \tag{24}$$

Where B is the condensation driving potential, $\overline{S}_m$ is the average Stanton number and G_m the average mass flux. So, it has been obtained again that the penetration length depends on the inverse of the driving potential B^{-1}, the inverse of the average Stanton number $\overline{S}_m^{-1}$ and $\left(\frac{G_0}{G_m}\right)$. Also, equation (24) shows that the penetration length increases with the initial mass flux, while diminishing with the DCC heat-transfer coefficient and with the pool subcooling.

An expression for the Stanton number is first needed to obtain the penetration length from equation (16) or (24). Several authors as Kim et al. (2001), Chun et al. (1996), Gulawani et al. (2006), and Wu et al. (2007) have obtained correlations for the average HTC, all of them can be expressed in terms of the Stanton number, as displayed in Table 1, the correlations were obtained using different exit nozzle diameters (D_0).

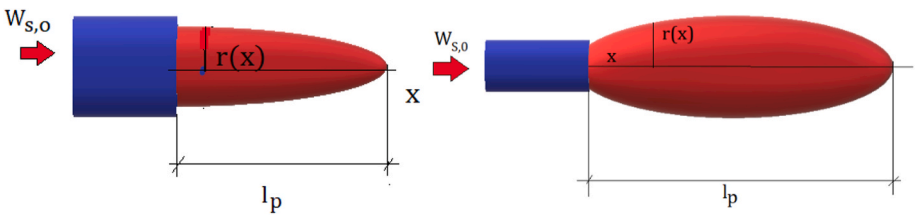

Fig. 3. Discharge of a) a hemi-ellipsoidal prolate jet and b) an ellipsoidal steam jet into a subcooled pool, both with steam penetration length l_p.

Table 1
Correlations for the transport modulus (Stanton number) of different authors for the discharge of steam jets in a subcooled pool.

Method	Correlation	References
Average HTC	$\frac{\bar{h}}{c_p G_{crit}} = 1.4453\, B^{0.03587}\left(\frac{G_0}{G_{crit}}\right)^{0.13315}$	Kim et al. (2001) $D_0 = 5mm, 7.1mm, 10.15mm, 15.5mm, 20mm$
Average HTC	$\frac{\bar{h}}{c_p G_m} = 1.3583 B^{0.0405}\left(\frac{G_0}{G_m}\right)^{0.3714}$	Chun et al. (1996) $D_0 = 1.35\ mm, 4.45\ mm, 7.65\ mm,$ 10.85 mm.
Average HTC	$\frac{\bar{h}}{c_p G_{crit}} = 1.12 B^{0.06}\left(\frac{G_0}{G_{crit}}\right)^{1.31}$	Gulawani et al. 2006 $D_0 < 2mm$
Average HTC	$\frac{\bar{h}}{c_p G_{crit}} = 1.54 B^{0.04}\left(\frac{G_0}{G_{crit}}\right)^{1.12}$	Gulawani et al. 2006 $D_0 > 6mm$
Average HTC	$\frac{\bar{h}}{c_p G_{crit}} = 0.576 B^{0.04}\left(\frac{G_0}{G_{crit}}\right)\left(\frac{p_f}{p_s}\right)^{0.2}$	Wu et al. (2007) $D_0 = 2.2\ mm, 3mm$

Substituting the expressions for the Stanton number into Kerney's expression, equation (16), or equation (24) for the ellipsoidal jet, one obtains a set of semi-empirical expressions for the dimensionless penetration length (X_p). Expression which is denoted as Kerney-Kim, if Kerney's equation is used for X_p and Kim's correlation for $\bar{S}_m$, or ellipsoidal-Chun if equation (24) is used, assuming an ellipsoidal shape for the jet and Chun's correlation for the Stanton number. The expressions obtained for Ellipsoidal-Chun and Kerney-Kim for the dimensionless penetration lengths $X_p = \frac{2l_p}{D_0}$ are:

$$X_p = 0.4686\, B^{-1.0405}\left(\frac{G_0}{G_m}\right)^{0.6286} - 0.6366 \tag{25}$$

$$X_p = 0.692\, B^{-1.03587}\left(\frac{G_0}{G_m}\right)^{0.3665} \tag{26}$$

Expression (25) provides an alternative correlation expression to Kerney's form, given by equation (17), which can be expressed as:

$$X_p = b_1\, B^{-b_2}\left(\frac{G_0}{G_m}\right)^{b_3} - b_4 \tag{27}$$

The fitting parameter values $b_i$of equation (27) have been obtained with the non-linear fitting program nlfit of MATLAB, using the 104 experimental data of Kerney for different diameters of the nozzle and different boundary conditions, the values of these fitting parameters are displayed in Table 2. Also, the experimental data of Kerney using the nlfit routine of MATLAB have been refitted obtaining a new correlation with smaller root mean square error (RMSE). Additionally, this table shows in the last column the RMSE error, which is used as a merit figure to compare the different correlations and semiempirical formulas:

$$RMSE = \sqrt{\frac{\sum_{i=1}^{N}\left(y_{th,i} - y_{exp,i}\right)^2}{N - p}} \tag{28}$$

Where N is the number of experimental points, p the number of fitting parameters, $y_{th,i}$ denote the theoretical values obtained with the correlation, and $y_{exp,i}$ the experimental values.

The results obtained for the RMSE with the different correlation and semiempirical formulas show us that the expressions based on equation (27) generally have a little bit less RMSE error than the expressions based on the Kerney type equation.

2.3. Condensation heat transfer coefficients (HTC) for steam jets

Fukuda (1982), and Simpson and Chan (1982) investigated the

Table 2
Comparison of different correlations and semiempirical formulas for $X_p$using Kerney Experimental data set and $G_{crit} = 275\frac{kg}{m^2 s}$.

Name	Method	$X_p = \frac{2l_p}{D_0}$	RMSE	References
Kerney Method	Kerney original equation	$0.7166\, B^{-0.8411}\left(\frac{G_0}{G_{crit}}\right)^{0.6466}$	2.6499	Kerney et al. (1972)
Kerney- refitted	Kerney data refitted with the nlfit program of MATLAB	$0.8463\, B^{-0.7671}\left(\frac{G_0}{G_{crit}}\right)^{0.6785}$	2.5816	
Kerney-Ellipsoidal	Expression from ellipsoidal jet shape and fitted coefficients from Kerney-data	$1.7692\, B^{-0.6309}\left(\frac{G_0}{G_{crit}}\right)^{0.5521} - 3.4663$	2.5777	
Ellipsoidal-Chun	Integration of the mass conservation equation assuming ellipsoidal jet form and Chun et al. correlation for the transport modulus	$0.4686\, B^{-1.0405}\left(\frac{G_0}{G_m}\right)^{0.6286} - 0.6366$	3.5963	
Kerney-Kim	Expression of Kerney with Kim et al. correlation for the transport modulus	$0.692\, B^{-1.03587}\left(\frac{G_0}{G_m}\right)^{0.3665}$	5.1778	
Kim et al. (1997)	Expression of Kim et al. for the pool at atmospheric pressure and $G_m = 275 kg/m^2 s$	$1.1846\, B^{-0.66}\left(\frac{G_0}{G_m}\right)^{0.344}$	6.176	Kim et al. (1997)
Kim et al. (2001)	Expression of Kim et al. for the dimensionless penetration length	$1.06\, B^{-0.70127}\left(\frac{G_0}{G_m}\right)^{0.47688}$	4.337	Kim et al. (2001)

interfacial heat transfer coefficient in DCC for steam discharges. They estimated a time average value of the heat transfer considering that the steam mass flow rate $W_s$into de bubble was constant and equal to the existing one at the vent discharge i.e., $W_s = \pi r_0^2 G_s$. In addition, Fukuda computed the heat transfer coefficient at the maximum radius attained by the bubble and assuming that the entering mass flow rate was equal to the condensing mass flow rate at this maximum radius, which as was obviously noticed by Gallego-Marcos et al. (2019) under-estimate the heat transfer coefficient. This simple calculation yields:

$$\pi r_0^2 G_s = \frac{\overline{h}\Delta T}{h_{fg}} 4\pi r_{max}^2 \Longrightarrow \overline{h} = \frac{\pi r_0^2 G_s h_{fg}}{4\pi r_{max}^2 \Delta T} \tag{29}$$

Then Fukuda measured the maximum radius with a high-speed camera and proposed the following correlation for the Nusselt number:

$$Nu = \frac{h d_v}{k_l} = 43.78 \left(\frac{d_v G_s}{\mu_l}\right)^{0.9} \frac{c_{p,l}\Delta T}{h_{fg}} \tag{30}$$

Where $\Delta T = T_s - T_\infty$, is the subcooling and the rest of the symbols are standard ones. Then Simpson and Chan (1982) performed the calculation of h performing an average of the interfacial area over a complete cycle of the bubble.

Gallego-Marcos et al. (2019) computed the heat transfer considering that during the time interval Δt, the spheroidal bubble size increases its volume ΔV_{elip} and therefore a portion of the incoming mass $\rho_s \Delta V_{elip}$ does not condense during this time interval. After detachment, the neck reduces its diameter andΔV_{elip} could become negative especially when $Q_b = 0$ i.e., when the bubble is completely detached. In general, the heat transfer coefficient (HTC) can be obtained from the expression:

$$h = \frac{\rho_s \left(Q_b \Delta t - \Delta V_{elip}\right) h_{fg}}{A_{i,elip}\ \Delta T} \tag{31}$$

where Q_b is the volumetric flow rate in m^3/s, which is equal to the steam volumetric flow rate $Q_{s,inj} = \pi r_0^2 v_{s,inj}$injected at the vent exit before the bubble detachment. After the detachment, Gallego-Marcos et al. (2019) found that the neck connecting the vent exit to the steam bubble was varying its size leading to a significant uncertainty in the determination of the volumetric flow rate Q_b to the steam. Therefore Gallego-Marcos et al. (2019) computed the HTC only for the detachment phase, and the correlation obtained for the Nusselt number is given by the expression:

$$Nu = \frac{\overline{h}\, d_v}{k_l} = 5.5\, Ja^{0.41} Re_s^{0.8} We^{-0.11} \tag{32}$$

where Ja is the Jakob non-dimensional number, Re the Reynolds number and We the Webber number. The definitions used for these numbers in equation (32) are:

$$Ja = \frac{c_{p,l}\Delta T}{h_{fg}},\ Re = \frac{G_s d_v}{\mu_s},\ We = \frac{\rho_s u_s^2 d}{\sigma} \tag{33}$$

Several authors have investigated the interfacial heat transfer coefficient in DCC during steam jet discharges, Chun et al. (1996) obtained that the average HTC depends on the steam mass flux G and the degree of pool subcooling $\Delta T_{sub} = T_{sat} - T_l$, increasing with G. These authors found that the average HTC, h_m was in the range of 1.0–3.5 $\frac{MW}{m^2 K}$. Otherwise, Kim et al. (2001) found that the average HTC was in the interval 1.24–2.05 $\frac{MW}{m^2 K}$. More information on the average heat transfer coefficient $\overline{h}$has been shown in Table 1.

3. Oscillations of discharged steam jets in subcooled water pools

3.1. Transition and condensation oscillations

The chugging oscillations (C), as displayed at Figs. 1 and 2, appear for low steam mass fluxes G and low pool water temperatures, and as the pool temperature increases the chugging oscillations occur at lower mass fluxes. As mentioned in the introduction, in the chugging region, the bubbles are formed outside the vent pipe and when attain a given size break up and condense so the pool water flow back penetrating into the vent discharging pipe (Wang et al., 2021). This process continues up to a limit length where the pressure exerted by the steam flux coming from the header pushes up all the liquid outside the vent, and the steam penetrates again into the pool forming a new bubble that when attains some size it breaks and collapses and the pool water again flows back to the vent, starting a new cycle, which is repeated periodically. In the transition region (TC), the oscillations are like the chugging ones except that the amplitude of the oscillations is smaller, and the water does not enter inside the vent line, and a cloud of small bubbles is formed near the vent exit. The other oscillations studied in this section are the condensation oscillations (CO) in these oscillations that take place at greater mass fluxes, the steam condensation occurs outside the vent nozzle and therefore the water does not enter inside the vent tube and the steam water interface oscillates violently (Hong et al., 2012). Finally, if the pool temperatures increase above 80 °C appear the so-called bubbling condensation oscillations (BCO) where the bubbles detach periodically with some characteristic frequency.

Arinobu (1980), Fukuda and Saitoh (1982), Aya and Nariai (1986), Zhao et al. (2016), Villanueva et al. (2015), Gallego-Marcos et al. (2019) performed several sets of experiments covering the following conditions: chugging (C), the transition to condensation oscillations (TC), the condensation oscillations (CO) and the bubbling (BCO). They also performed experiments to try to predict the temperature subcooling thresholds for the appearance of the low frequency and the high frequency oscillations. They found experimentally (Aya and Nariai 1986) that for high frequency oscillations the temperature-subcooling threshold ΔT_{THf}disminishes with the mass flux, however for low-frequency oscillations Arinobu (1980) found that the temperature subcooling threshold $\Delta T_{TLf}$was practically constant with the steam mass flux.

In this section, the models of Fukuda and Saitoh (1982) and Aya and Nariai (1986) are reviewed, but instead of a spherical or a cylindrical model an ellipsoidal jet model has been used. Additionally, a comparison of the new results with these of previous models and with the experimental data has been carried out, also discussing the best way to improve their predictions. Finally, it has been found that especially useful to improve the results are the correlations obtained by Gallego--Marcos et al. (2019).

A model like the one used by Aya and Nariai (1986) is considered, but with a prolate hemi-ellipsoidal shape for the steam-jet. The steam bubble is assumed to have an ellipsoidal shape, as displayed at Fig. 4,

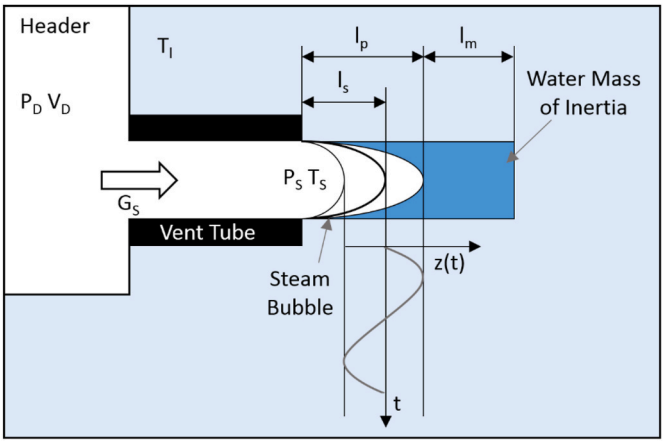

Fig. 4. Model for the discharge of a steam mass flow rate into a pool a temperature T_l thought a discharge pipe or vent of diameter $d_v = 2r_0$, assuming a hemi-ellipsoidal shape for the steam discharge.

with penetration length $l_p(t)$ that oscillates around the value l_s, being $z(t)$ the variation with time of the length of the oscillations around the average penetration value, so it can be written:

$$l_p(t) = l_s + z(t) \tag{34}$$

Where according to Fig. 4 $z(t)$ can be positive or negative. It is assumed that the inertial effect of the pool water against the interfacial motion is represented by all the water contained inside the cylinder of length l_m, plus the amount of water contained in the volume of the cylinder of length l_p minus the volume of the hemi-ellipsoid as displayed at Fig. 4.

For small mass fluxes, the steam does not penetrate too much, and the shape of the bubble is spherical as assumed by Fukuda and Saitoh (1982) or conical. For bigger jet lengths, it can be assumed to have cylindrical or hemi-ellipsoidal shapes.

The mass conservation equation for the steam volume $V_s$can be written as follows:

$$\frac{d}{dt}(V_s(t)\rho_s) = \frac{\pi}{4} d_v^2 G_s - \frac{\overline{h}\Delta T}{h_{fg}} A_i(t) \tag{35}$$

Where $V_s(t)$ is the steam volume, and $A_i(t)$ denotes the interfacial area of the steam with the surrounding liquid. The expression for both magnitudes can be written in terms of the penetration length $l_p(t)$ of the jet in the water pool as:

$$V_s(t) = V_0 + \frac{2}{3}\pi r_0^2 l_p(t) \tag{36}$$

$$A_i(t) \cong \frac{\pi^2}{2} r_0 l_p(t) + \pi r_0^2 \tag{37}$$

The volume V_0 in equation (36) is the volume of the header V_D plus the volume of the vent tube, the second term is the volume of a half prolate-spheroid. The interfacial area expression has been obtained from equation (23).

If the steam is at saturated conditions or close to them then $\rho_s = \rho_s(p)$ and on account that the pressure changes with time, then operating in equation (35) yields:

$$\rho_s \frac{d}{dt} V_s(t) + V_s(t) \frac{\partial \rho_s}{\partial p_s} \frac{dp_s}{dt} = \frac{\pi}{4} d_v^2 G_s - \frac{\overline{h}\Delta T}{h_{fg}} A_i(t) \tag{38}$$

Assuming that the oscillations of the physical magnitudes are performed around an equilibrium value denoted by the subindex 0, then one may write:

$$p_s(t) = p_{s,0} + \delta p_s(t) \tag{39}$$

$$\Delta T = T_s(t) - T_l = \Delta T_0 + \delta \Delta T(t) = \Delta T_0 + \delta T_s(t) \tag{40}$$

The fluctuations in the difference of temperature between the steam and the liquid pool are related to the fluctuations of temperature of the steam and are given by:

$$\delta T_s = \frac{\partial T_s}{\partial p_s} \delta p_s \tag{41}$$

The fluctuation in δp_s are governed considering the Newton law and the inertial mass displayed at Fig. 4, by the equation:

$$\pi r_0^2 \delta p_s = \rho_l V_{inertia} \frac{d^2 z}{dt^2} \tag{42}$$

where the inertial volume displayed at Fig. 4 in dark blue color is given by the expression:

$$V_{inertia} = \pi r_0^2 l_m + \frac{1}{3}\pi r_0^2 l_p(t) \tag{43}$$

From equations (42) and (43), it is obtained after some simplifications:

$$\delta p_s = \rho_l \left(l_m + \frac{1}{3}(l_s + z(t)) \right) \frac{d^2 z}{dt^2} \tag{44}$$

Therefore, the pressure change with time is governed by the equation:

$$\frac{dp_s}{dt} = \frac{d\delta p_s}{dt} = \rho_l \left(l_m + \frac{1}{3}(l_s + z(t)) \right) \frac{d^3 z(t)}{dt^3} + \rho_l \frac{1}{3} \frac{dz}{dt} \frac{d^2 z}{dt^2} \tag{45}$$

The oscillations in $l_p(t)$take place around the equilibrium value l_s, and at equilibrium conditions, equation (38) reduces to:

$$\frac{\pi}{4} d_v^2 G_s - \frac{\overline{h}\Delta T_0}{h_{fg}} A_{i,o} = \frac{\pi}{4} d_v^2 G_s - \frac{\overline{h}\Delta T_0}{h_{fg}} \left(\frac{\pi^2}{2} r_0 l_s + \pi r_0^2 \right) = 0 \tag{46}$$

Subtracting equation (46) from equation (38) yields because of equation (40):

$$\rho_s \frac{d}{dt} V_s(t) + V_s(t) \frac{\partial \rho_s}{\partial p_s} \frac{dp_s}{dt} = -\frac{\overline{h}\Delta T_0}{h_{fg}} \frac{\pi^2}{2} r_0 z(t) - \frac{\overline{h}\,\delta \Delta T}{h_{fg}} A_i(t) \tag{47}$$

Then considering equations (41) and (44)–(46), in equation (47) it is obtained after some calculus and algebra the following equation for the evolution of $z(t)$, where only the linear terms in z(t) and their derivatives are explicitly displayed:

$$\frac{d^3 z}{dt^3} + A \frac{d^2 z}{dt^2} + B \frac{dz}{dt} + \mathrm{C}\ \mathrm{z} + \mathrm{non} - \mathrm{linear\ terms} = 0 \tag{48}$$

The coefficients of the linear terms in equation (48) are given by:

$$A = \frac{\overline{h}}{h_{fg}} \frac{\left(\frac{\pi^2}{2} r_0 l_s + \pi r_0^2 \right)}{\left(V_0 + \frac{2}{3}\pi r_0^2 l_s \right)} \left(\frac{\partial T_s}{\partial \rho_s} \right) = \frac{\overline{h}}{h_{fg}} \frac{A_{i,0}}{V_{s,0}} \left(\frac{\partial T_s}{\partial \rho_s} \right) \tag{49}$$

$$B = \frac{\rho_s}{\rho_l} \frac{\frac{2}{3}\pi r_0^2}{\left(V_0 + \frac{2}{3}\pi r_0^2 l_s \right)\left(l_m + \frac{1}{3} l_s \right)} \frac{\partial p_s}{\partial \rho_s} \tag{50}$$

$$C = \frac{\overline{h}\Delta T_0}{h_{fg}\rho_l} \frac{\pi^2 r_0}{\left(V_0 + \frac{2}{3}\pi r_0^2 l_s \right)\left(l_m + \frac{1}{3} l_s \right)} \frac{\partial p_s}{\partial \rho_s} \tag{51}$$

Equation (48) can be converted to a non-linear ordinary differential equation system, by performing the changes of variables $\dot{z} = z_1, \dot{z}_1 = z_2$, the linear part of this ordinary differential equation system is:

$$\frac{d}{dt} \begin{pmatrix} z \\ z_1 \\ z_2 \end{pmatrix} = \begin{pmatrix} 0 & 1 & 0 \\ 0 & 0 & 1 \\ -C & -B & A \end{pmatrix} \begin{pmatrix} z \\ z_1 \\ z_2 \end{pmatrix} = [J] \begin{pmatrix} z \\ z_1 \\ z_2 \end{pmatrix} \tag{52}$$

Considering that the system stability is determined by the Lyapunov exponents of the linear part (Guckenheimer and Holmes 1986), which are the eigenvalues of the Jacobian Matrix of the system at the equilibrium point, which are obtained as it is well known by solving the equation:

$$\begin{vmatrix} 0-\lambda & 1 & 0 \\ 0 & 0-\lambda & 1 \\ -C & -B & A-\lambda \end{vmatrix} = 0 \Rightarrow \lambda^3 + A\lambda^2 + B\lambda + C = 0 \tag{53}$$

Because of the general solution of equation (52) can be obtained by a linear superposition of 3 linearly independent solutions if the matrix $[J]$ has three linearly independent eigenvectors $\boldsymbol{v}^{(j)}$. Then the general solution of the linear problem can be expressed in the form (Guckenheimer and Holmes 1986):

$$z(t) = \sum_{j=1}^{3} c_j \boldsymbol{v}^{(j)} e^{\lambda_j t} \tag{54}$$

Therefore, the linear system is stable is $Re\,\lambda_j < 0\,, j = 1,2,3$, and unstable if $Re\,\lambda_j > 0$for $j = 1,2,3$. By the Hartman-Grobman theorem (Guckenheimer and Holmes 1986, Muñoz-Cobo and Verdú, 1991), the system stability can be extended to the entire system including the

non-linear part, with the condition that the real parts of all the eigenvalues of the Jacobian Matrix $[J]$ at the equilibrium point are $\neq 0$.

The system stability can be obtained by applying the Routh Hurwitz criterium to the characteristic equation (53) (D'Azzo and Houpis, 1988). Application of this criterium yields:

$$\begin{array}{c|cc} \lambda^3 & 1 & B \\ \lambda^2 & A & C \\ \lambda^1 & (AB-C)/A & . \\ \lambda^0 & C & . \end{array} \tag{55}$$

To be stable, the sign of all the terms of the first column must be the same, in this case positive therefore, $A > 0, C > 0$ *and* $AB > C$, therefore for stability it also follows that $B > 0$. Therefore, the threshold for stability is given according to this criterium by the condition:

$$AB = C \tag{56}$$

From equation (56) because of equations (49)–(51), it is obtained after some simplifications the following expression for the subcooling at the oscillation threshold when the jet shape is hemi-ellipsoidal as displayed at Fig. 3:

$$\Delta T_{TLf} = \frac{l_s + \frac{d_v}{\pi}}{l_s + \frac{V_0}{\pi \frac{d_v^2}{6}}} \rho_s \frac{\partial T_s}{\partial \rho_s} \tag{57}$$

Pressure oscillations of low frequency start when the water pool subcooling ΔT exceeds the threshold subcooling given by equation (57). Low and high frequency pressure-oscillations can exist, according to Aya and Nariai (1986), the lower ones are controlled by the steam volume of the header plus the vent and the volume of the jet-steam i.e. $V_0 + \frac{2}{3}\pi r_0^2 l_s$, while the high frequency pressure oscillations are controlled only by the steam jet volume $\frac{2}{3}\pi r_0^2 l_s$.

The threshold subcooling for high frequency oscillations is obtained by setting $V_0 = 0$ in equation (57) that yields:

$$\Delta T_{THf} = \frac{l_s + \frac{d_v}{\pi}}{l_s} \rho_s \frac{\partial T_s}{\partial \rho_s} \tag{58}$$

Fukuda (1982) and Aya and Nariai (1986) obtained expressions for the subcooling thresholds, which are shown in Table 3.

To obtain the subcooling threshold with the different models, it is needed to compute two magnitudes the first one is the partial derivative $\frac{\partial T_s}{\partial \rho_s}$ and the second one the steam penetration length. To compute $\frac{\partial T_s}{\partial \rho_s}$, it is assumed that the process is polytropic because most of the thermodynamic process of practical interest are polytropic with coefficient n varying between $1 \leq n \leq 1.3$ for water steam. For a polytropic process it holds:

$$T_s \left(\frac{1}{\rho_s}\right)^{n-1} = cte \Rightarrow \frac{\partial T_s}{\partial \rho_s} = (n-1)\frac{T_s}{\rho_s} \tag{59}$$

For polytropic processes with wet steam that suffer expansions and contractions the polytropic index is ranging in the interval $1.08 \leq n \leq 1.2$ depending on the characteristics of the process (Soh and Karimi 1996; Romanelli et al., 2012), we have chosen the values of $n = 1.07, 1.082, 1.09$ to perform the calculations. For high temperatures of the liquid, close to 90 °C, when the steam condensation diminishes the polytropic coefficient approach to 1.3.

To obtain the steam penetration length l_s, it is performed a mass balance between the injected mass flow rate and the condensed mass flow rate, which yields for the spheroid-prolate case:

$$\pi r_0^2 G_s = \frac{\overline{h}\Delta T}{h_{fg}} A_i = \frac{\overline{h}\Delta T}{h_{fg}} \left(\frac{\pi^2}{2} r_0 l_s + \pi r_0^2\right) \Rightarrow l_s = \frac{d_v}{\pi}\left(\frac{G_s h_{fg}}{\overline{h}\Delta T} - 1\right) \tag{60}$$

To compute $\overline{h}$ in equation (60) we have used the HTC deduced from Gallego-Marcos et al. (2019) correlation for the Nusselt number, and which is given by equation (32).

Table 3
Subcooling threshold for low and high frequency oscillations in discharges of steam in subcooled pools.

Name	Jet Shape	Subcooling Threshold
Fukuda-low frequency oscillations	Spherical	$\Delta T_{TLf} = \frac{2\pi r^3}{V_0 + \frac{4}{3}\pi r^3} \rho_s \frac{\partial T_s}{\partial \rho_s}$
Fukuda-high frequency oscillations	Spherical	$\Delta T_{THf} = \frac{3}{2} \rho_s \frac{\partial T_s}{\partial \rho_s}$
Aya-and Nariai-low frequency oscillations	Cylindrical	$\Delta T_{TLf} = \frac{l_s + \frac{d_v}{4}}{l_s + \frac{V_0}{\left(\frac{\pi d_v^2}{4}\right)}} \rho_s \frac{\partial T_s}{\partial \rho_s}$
Aya-and Nariai-High frequency oscillations	Cylindrical	$\Delta T_{THf} = \frac{l_s + \frac{d_v}{4}}{l_s} \rho_s \frac{\partial T_s}{\partial \rho_s}$
This paper-Low frequency oscillations	Hemi-ellipsoidal (Spheroid-prolate)	$\Delta T_{TLf} = \frac{l_s + \frac{d_v}{\pi}}{l_s + \frac{V_0}{\pi \frac{d_v^2}{6}}} \rho_s \frac{\partial T_s}{\partial \rho_s}$
This paper-High frequency oscillations	Hemi-ellipsoidal (Spheroid-prolate)	$\Delta T_{THf} = \frac{l_s + \frac{d_v}{\pi}}{l_s} \rho_s \frac{\partial T_s}{\partial \rho_s}$

3.2. Results for the transition (TCO), condensation oscillations (CO), and bubbling condensation oscillations (BCO)

Experimental data for the subcooling threshold for high frequency oscillations ΔT_{THf} with different mass fluxes were obtained by Fukuda and Saitoh (1982) and by Aya and Nariai (1986). The results for this case, as shown in Table 3, depends on the penetration length l_s, the vent diameter d_v, and the product of the steam density and the partial derivative $\frac{\partial T_s}{\partial \rho_s}$, which for polytropic processes, because of equation (59), depends on the polytropic exponent n. Also to obtain l_s, because of equation (60), it is necessary to know the average heat transfer coefficient. These experiments clearly show as displayed in Fig. 5 that the subcooling thresholdΔT_{THf} diminish with the steam mass flux G_s. However, using the correlation obtained by Fukuda (1982), the result is that ΔT_{THf} is practically constant.

If the correlation for the Nusselt number deduced by Gallego-Marcos et al. (2019) and given by equation (32) is used, instead of the correlation used by Fukuda and Saitoh (1982). First, it is observed that the Gallego-Marcos et al. correlation depends on the subcooling and second the expression (60) used to obtain the penetration length depends also on the subcooling and $\overline{h}$, therefore the resulting equation is a non-linear algebraic equation in ΔT, of the standard form x = f(x) and given by:

$$\Delta T = \left[1 + \frac{C_1 k_l(T_l)\Delta T^{1.41}}{G_s h_{fg} - C_1 k_l(T_l)\Delta T^{1.41}}\right] \rho_s \frac{\partial T_s}{\partial \rho_s} \tag{61}$$

Where the coefficient C_1 is given by:

$$C_1 = \frac{5.5}{d_v}\left(\frac{c_{pl}}{h_{fg}}\right)^{0.41} Re_s^{0.8}\, We^{-0.11} \tag{62}$$

The algebraic equation (61) has been solved by iterations, normally

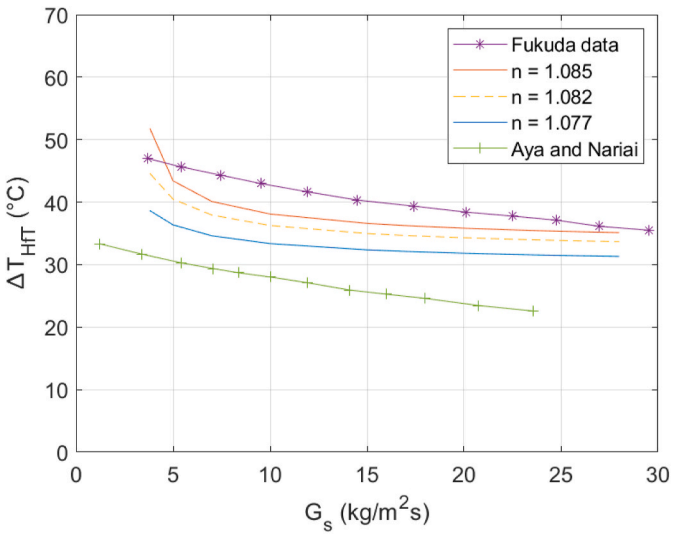

Fig. 5. Subcooling threshold ΔT_{THf} for high-frequency oscillations computed using equation (61), with the correlation of Gallego-Marcos et al. (2019), three values $n = 1.077, 1.082, 1.085$ of the polytropic coefficient and $d_v = 16\ mm$. Comparison with the experimental data of Fukuda (1982) and Aya and Nariai (1986).

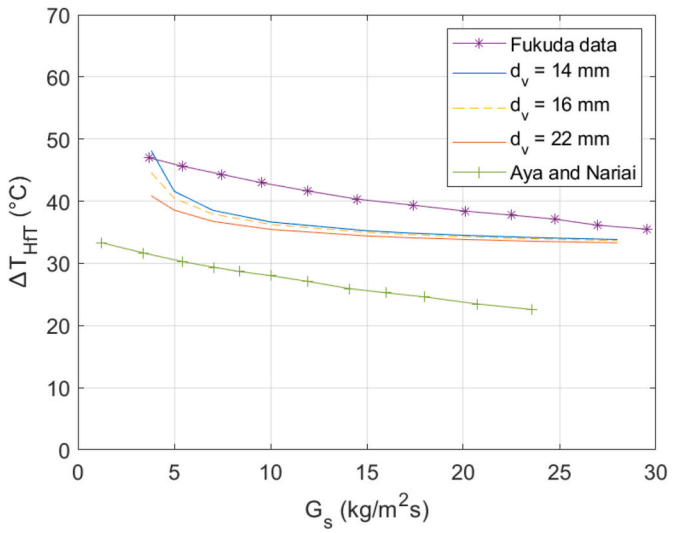

Fig. 6. Subcooling threshold ΔT_{THf} for the high-frequency oscillations computed using equation (61), and the correlation of Gallego-Marcos et al. (2019), $n = 1.082$, and three vent diameters $d_v = 14, 16, 22\ mm$. Comparison with the experimental data of Fukuda (1982) and Aya and Nariai (1986).

few iterations are needed for convergence, usually less than 10. In some cases, particularly for low mass flux values smaller than $5\ kg/\ m^2s$, the Newton method has been used, since gives better convergence. Also, it is noticed that the subcooling values obtained when varying the mass flux are dependent on the polytropic coefficient n. Fig. 5 displays the high frequency subcooling threshold computed with three different values n = 1.077, n = 1.082 and = 1.085 of this coefficient, and with a vent diameter $d_v = 16\ mm$. Also, notice that it has been observed that for all these values of the polytropic coefficient, the calculated subcooling thresholds are located between the experimental values obtained by Aya and Nariai and those obtained by Fukuda. However, for n = 1.085 there is one point that is a little bit above the experimental data, as displayed at Fig. 5.

Because of Fukuda and Saitosh's expression for the subcooling threshold ΔT_{Hfr} is independent on the steam mass flux G_s, as it is deduced considering Table 3. We have deduced that the polytropic exponent used by Aya and Nariai (1986) to predict a threshold value of $\Delta T_{THf} = 44.3$ K using Fukuda expression is:

$$\Delta T_{THf} = 44.3 = \frac{3}{2}(n-1)T_s \Longrightarrow n = 1.079 \tag{63}$$

So, the polytropic coefficient is close to 1.08, and with this coefficient the model predictions given by equation (61) are close and a little bit below the curve denoted as $n = 1.082$ in Fig. 5.

Also, from Fig. 5 it is observed that the subcooling threshold predicted by equation (61) diminish with the mass flux G_s as observed experimentally. However, for high mass fluxes the slope of the curve becomes smaller than the experimental one and for small mass fluxes becomes bigger.

The results for the predicted subcooling threshold depend slightly on the vent diameter, we have performed the calculations with three different diameters $d_v = 12\ mm$, $d_v = 16\ mm$ and $d_v = 22\ mm$, and the results are displayed at Fig. 6. These results are also compared with the experimental data of Fukuda and Aya and Nariai. It is observed that the model predicts that the subcooling threshold diminishes when the vent diameter increases.

Next, the liquid temperature threshold for the occurrence of low frequency oscillation components in the discharges of steam into a subcooled water pool will be discussed. Experimentally this case has been studied by Arinobu (1980), Chan and Lee (1982), Aya and Nariai (1986). As was discussed by different authors as, Aya and Nariai (1986), the low frequency components of the oscillations is controlled by a larger steam volume, which includes the header and the section of pipe from the header to the discharge vent, in the case of the experiments performed by Chan and Lee (1982) the header volume was 0.044 m^3, in the case of Aya and Nariai this volume ranges from 0.005 to 0.04 m^3. The equation used to predict the subcooling threshold for low frequency oscillations is equation (57), substituting in this equation the expression for the penetration length given by equation (60) and because of the expression for the heat transfer coefficient obtained by Gallego-Marcos et al. (2019), given by equation (32), it is obtained after some calculus the following equation for the low frequency subcooling threshold denoted by ΔT_{TLf}:

$$F(\Delta T_{TLf}) = C_2\left(\frac{6V_0}{d_v^3}\right)\Delta T_{TLf}^{2.41} + G_s h_{fg}\Delta T_{TLf} - G_s h_{fg}\rho_s \frac{\partial T_s}{\partial \rho_s} = 0 \tag{64}$$

Where C_2 is given by:

$$C_2 = C_1 k_l = \frac{5.5 k_l}{d_v}\left(\frac{c_{pl}}{h_{fg}}\right)^{0.41} Re_s^{0.8}\ We^{-0.11} \tag{65}$$

Equation (64) has been solved by the following Newton iteration algorithm that converges very fast for the analyzed cases:

$$\Delta T_{TLf}^{(r+1)} = \Delta T_{TLf}^{(r)} - \frac{F(\Delta T_{TLf})}{F'(\Delta T_{TLf})} \tag{66}$$

Denoting by the supra-index r the subcooling result of the r-th iteration and being $F'(\Delta T_{TLf})$ the derivative of the function $F(\Delta T_{TLf})$, with respect to the subcooling. For this case of low subcooling the polytropic exponent should be closer to the adiabatic value of 1.3, and then this value has been taken for the calculations. For the volume of the header plus the pipes, a volume $V_0 = 0.04768 m^3$ has been chosen, as suggested by Lee and Chan (1980). In Fig. 7, it is represented the liquid temperature threshold for low frequency oscillation versus the mass flux obtained solving equation (64), with the previous data and a vent discharge diameter of $d_v = 50.8\ mm$. It is observed that both curves are very close and the variation of the slope with G_S is practically the same.

It is convenient to analyze the sensitivity of the low frequency temperature threshold $T_{l,TLf}$ to the vent discharge diameter d_v and to the polytropic coefficient n. This threshold $T_{l,TLf}$ was computed for three

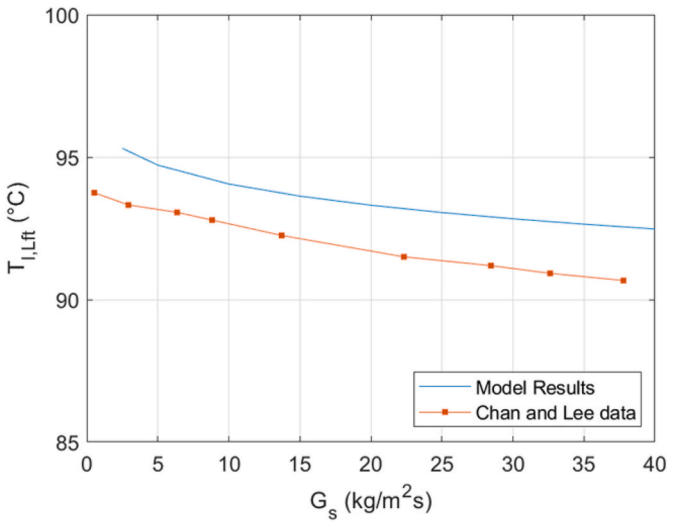

Fig. 7. Liquid temperature threshold$T_{l,TLf} = 100 - \Delta T_{TLf}$ for low frequency pressure oscillations for steam condensation in pool water versus gas flux according to Chan and Lee data (1982). The model results were calculated with the facility data $d_v = 50.8\,mm$, $V_0 = 0.04768\,m^3$ and a polytropic coefficient value of $n = 1.3$.

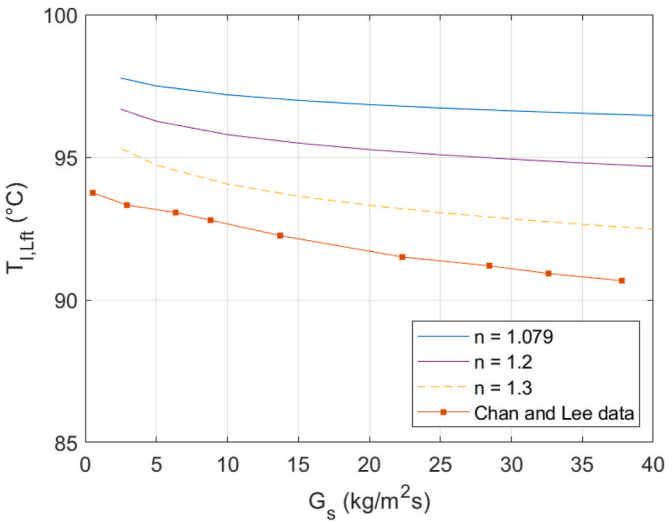

Fig. 9. Liquid temperature threshold$T_{l,TLf}$ for low frequency pressure oscillations for steam condensation in pool water versus the gas flux according to Chan and Lee data (1982). The model results were calculated with three polytropic values $n = 1.079, 1.2, 1.3$, $V_0 = 0.04768\,m^3$ and a vent diameter $d_v = 50.8\,mm$ as in Chan and Lee experiment.

different vent diameters ($d_v = 45.8, 50.8, 55.8\,mm$) and three different values of the polytropic coefficient ($n = 1.079, 1.2, 1.3$). In addition, these results were compared with the experimental data of Chan and Lee (1982).

Fig. 8 displays the results obtained solving equation (64) for different vent diameters. It is observed that the experiment of Chan and Lee was performed with a vent diameter of 50.8 mm, and the model results that are closer to the experimental data are the ones obtained with a vent diameter of 55.8 mm displayed with violet color, while the more distant ones are the computed with a vent diameter of 45.8 mm. Therefore, increasing the vent discharge diameter tends to diminish the liquid temperature threshold for low frequency oscillations.

Also, Fig. 9 displays, the threshold temperatures for low frequency pressure oscillations, computed with three different values of the polytropic coefficient ($n = 1.079, 1.2, 1.3$). It is observed that the results that are closer to the experimental values are the ones obtained with the polytropic coefficient of 1.3. This is a logic consequence of the fact that when increasing the pool temperature, and this temperature is close to saturation conditions, the heat exchange at the interface decreases and the process tends to be an adiabatic process with a polytropic coefficient value close to 1.3.

To finish this section, Fig. 10 displays the results obtained solving equation (64) and then computing the liquid temperature threshold $T_{l,TLf} = 100 - \Delta T_{l,TLf}$ for low frequency oscillations. Additionally, Fig. 10 compares these results with the ones measured by Chan and Lee (1982) and Cho et al. (1998) (Figs. 1 and 2). The results show that for steam mass fluxes smaller than 50 kg/m^2s, the model results are closer to the experimental data of Chan and Lee and for mass fluxes higher than 75 kg/m^2s, the model results are closer to the data of Cho et al. and for higher fluxes practically match these last data as shown in Fig. 10.

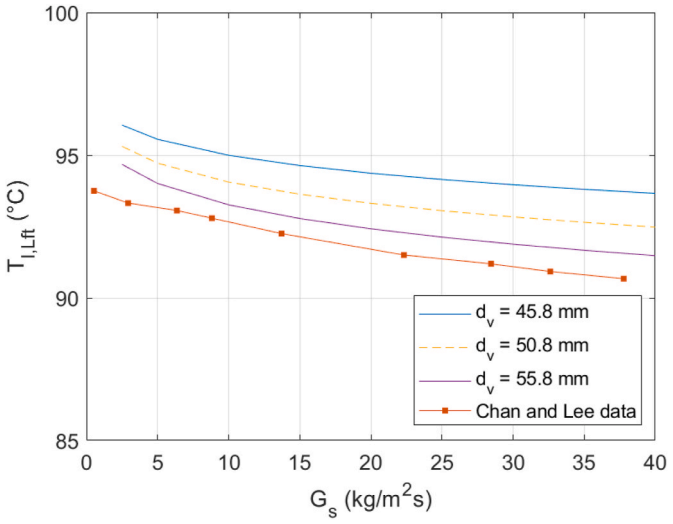

Fig. 8. Liquid temperature threshold$T_{l,TLf}$ for low frequency pressure oscillations for steam condensation in pool water versus gas flux according to Chan and Lee data (1982). The model results were calculated with three vent diameters $d_v = 45.8, 50.8, 55.8\,mm$, $V_0 = 0.04768\,m^3$ and a polytropic coefficient value of $n = 1.3$.

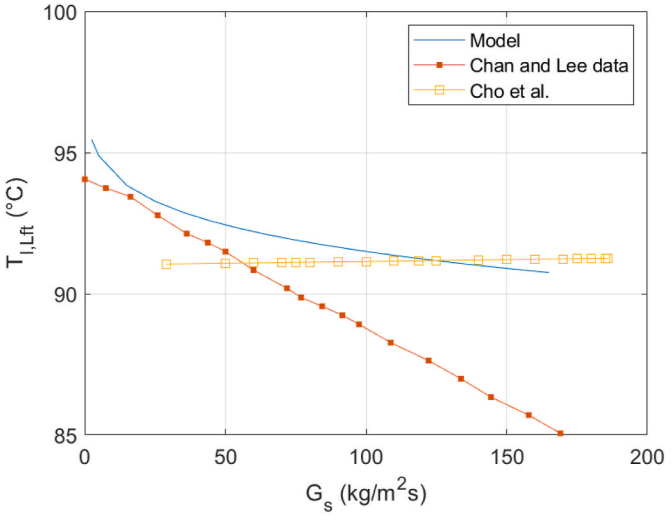

Fig. 10. Liquid temperature threshold$T_{l,TLf}$ for low frequency pressure oscillations of a condensing jet of steam in pool water versus the gas flux according to Chan and Lee data (1982) and Cho et al. data (1998). Current model results for$T_{l,TLf}$ were computed with n = 1.3, $V_0 = 0.04768\,m^3$ and a vent diameter $d_v = 50.8\,mm$ as in Chan and Lee experiment.

3.3. Oscillations in the SC and IOC map regions

3.3.1. Extension of Hong et al. model to include entrainment in the liquid region

At first, the modelling of the oscillations in the SC and IOC regions, follows the method developed by Hong et al. (2012). In addition, the modelling also considers the effect produced by the liquid entrainment in the liquid dominant region, as displayed in Fig. 11. This section also discusses the model characteristics that can be improved to consider the new contributions. Zhao et al. (2016) performed experiments in this region with mass fluxes ranging from 300 to 800 kg/m^2s, and subcooling of pool water (ΔT) ranging from 40 to 80 °C, which means that the experiments were in the right-hand side regimes of Fig. 1.

Hong's model assumes that the jet is formed by two regions, a steam dominated region (SDR) where the steam condenses and attains an average penetration length denoted by X, and a liquid dominated region (LDR). In addition, we have assumed in this paper that in the LDR region, the liquid jet entrains mass from the ambient fluid, and the entrainment velocity $u_e(x)$ is proportional to the liquid jet average velocity $u_l(x)$:

$$u_e(x) = \alpha_E \sqrt{\frac{\rho_l}{\rho_a}} u_l(x) \tag{67}$$

Being α_E the entrainment coefficient, that for a jet has a value ranging from$\alpha_E = 0.0522$ to$\alpha_E = 0.065$ (Rodi 1982; Papanicolaou and List, 1988; Harby et al., 2017), $\rho_a$is the ambient density that is the pool density, which is close to the jet density in the LDR region, so $\sqrt{\rho_l/\rho_a}$ is close to 1.

Due to the liquid entrained, the continuity equation in the LDR region can be written as:

$$\frac{\partial}{\partial x}(A(x)u_l(x)) = \frac{\pi \alpha_E}{\cos\beta} d_2(x) u_l(x) \tag{68}$$

Being $A(x)$ the transverse area of the jet in the LDR region, β the expansion angle of the jet in the LDR region, and $d_2(x)$ the jet diameter.

Hong et al.'s mechanistic model is based on the simple assumption that the work ($Work_{sl}$)performed by the steam against the liquid region as the vapor region expands is given to the ambient liquid as kinetic energy (KE_l). Additionally, considering equation (68), the liquid region expands due to the liquid entrained as displayed at Fig. 4. In this model the liquid entrained in the mixing region is neglected, because this region is small compared to the liquid dominant region.

In addition, the model also assumes: i) that the effective diameter of the liquid region at a distance x measured from the vent discharge is proportional to this distance, i.e., $d_2(x) = k_2\, x$, being k_2 the jet expansion coefficient in the LDR region. The same assumption is performed concerning the effective diameter of the vapor or steam in the SDR region, therefore at the frontier between the two regions it is assumed that the effective diameter is $d_l(X) = k_l X$; ii) the model also assumes that the velocity in the liquid region can be represented by an average velocity denoted by $u_l(x)$; iii) in addition the model considers that the entrained water does not affect the total kinetic energy KE_l transferred to the liquid but affect to the local velocity because the entrained mass increases the amount of mass in the jet so its velocity must diminish accordingly; iv) It is assumed that the velocity of entrainment at the liquid boundary depends on the average velocity of the jet in the LDR region.

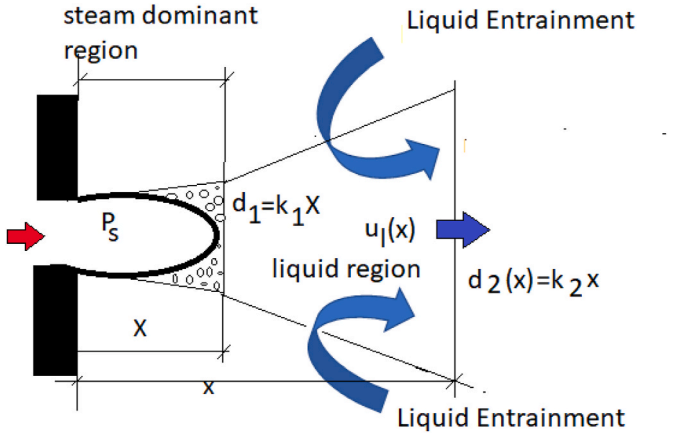

Fig. 11. Modelling of submerged steam jet with entrainment in the liquid region.

First, integrating the liquid mass conservation equation (68) between the boundary X and x yields:

$$A(x)u_l(x) - A(X)\frac{dX}{dt} = \frac{\pi \alpha_E}{\cos\beta}\int_X^x d_2(x')u_l(x')dx' \tag{69}$$

Equation (69) has been solved by perturbation theory considering the solution of order zero as the solution without entrainment in the liquid region, i.e., proceeding in this way when $\alpha_E = 0$ is taken, the solution obtained by Hong et al. (2012) is recovered. From equation (69) it follows:

$$u_l(x) = \frac{A(X)}{A(x)}\frac{dX}{dt} + \varepsilon\frac{\pi \alpha_E}{\cos\beta}\int_X^x d_2(x')u_l(x')dx' \tag{70}$$

Where ε is the order parameter that is set to 1 according to the perturbation method. Next, we set in equation (69):

$$u_l(x) = u_l^{(0)}(x) + \varepsilon u_l^{(1)}(x) + \varepsilon^2 u_l^{(2)}(x) + \ldots \tag{71}$$

The zero order and first order terms of the solution are:

$$u_l^{(0)}(x) = \frac{A(X)}{A(x)}\frac{dX}{dt} = \frac{(K_l X)^2}{(K_2 x)^2}\frac{dX}{dt} \tag{72}$$

and

$$u_l^{(1)}(x) = \frac{1}{A(x)}\frac{\pi \alpha_E}{\cos\beta}\int_X^x d_2(x')u_l^{(0)}(x')dx' = \frac{1}{A(x)}\frac{\pi \alpha_E}{\cos\beta}\frac{dX}{dt}\frac{(k_l X)^2}{(k_2)^2}\log\left(\frac{x}{X}\right) \tag{73}$$

Therefore, the first-order solution when entrainment in the LDR is considered is given by the expression:

$$u_l(x) = \frac{(k_l X)^2}{(k_2 x)^2}\frac{dX}{dt} + \frac{4\alpha_E}{\cos\beta}\frac{dX}{dt}\frac{(k_l)^2}{(k_2)^4}\frac{\log\left(\frac{x}{X}\right)}{\left(\frac{x}{X}\right)^2} \tag{74}$$

The next step is to obtain the work performed by the steam against the liquid region as the vapor region expands, $Work_{sl}$, this work can be expressed as obtained by Hong et al. (2012) as follows:

$$Work_{sl} = \frac{\pi}{12}k_l^2 X^3 (P_s - P_\infty) \tag{75}$$

Being P_s the steam pressure of the SDR region and P_∞ the pressure of the LDR region. The kinetic energy given to the liquid region is computed by performing the following integral over the volume of the LDR region:

$$KE_l = \int_{V_{LDR}} \frac{1}{2}\rho_l u_l^2(x)dV(x) = \int_X^\infty \frac{1}{2}\rho_l u_l^2(x)\frac{\pi(k_2 x)^2}{4}dx \tag{76}$$

Direct substitution of the velocity expression given by equation (74) in equation (76), yields after some calculus:

$$KE_l = \frac{\pi}{8}\rho_l\left(\frac{dX}{dt}\right)^2\frac{k_l^4}{k_2^2}X^3\left(1 + \frac{8\alpha_E}{\cos\beta\, k_2^2} + \frac{1}{2}\left(\frac{8\alpha_E}{\cos\beta\, k_2^2}\right)^2\right) \tag{77}$$

Equating the work performed by the steam during the expansion to the kinetic energy gained by the liquid and performing the derivative of the result with respect to time yields, after some calculus, the following result:

$$X\frac{d^2X}{dt^2}+\frac{3}{2}\left(\frac{dX}{dt}\right)^2-\frac{1}{\rho_l}\left(\frac{k_2}{k_1}\right)^2\frac{(P_s-P_\infty)}{\left(1+\frac{8\alpha_E}{\cos\beta\,k_2^2}+\frac{1}{2}\left(\frac{8\alpha_E}{\cos\beta\,k_2^2}\right)^2\right)}=0 \tag{78}$$

Equation (78) is the "jet equation with entrainment in the LDR region", which reduces to Hong et al. (2012) "jet equation" when no entrainment is considered ($\alpha_E = 0$). Equation (78) has a form that resembles to the Rayleigh-Plesset equation (Plesset, 1949) for the bubble dynamics (Moody 1990) except the last term, where the difference comes from the factor $\left(\frac{k_2}{k_1}\right)^2$ and the entrainment term. About this equation, for a bubble Moody (1990), says that a compressible steam bubble resembles a spring and the surrounding ambient liquid a mass. Therefore, performing a small compression and release of a gas bubble, which is initially in mechanical equilibrium with the surrounding liquid would start an oscillation. This situation can be extended to a jet if initially is in equilibrium with $X = X_{eq}$, and this equilibrium initial jet length X_{eq} is perturbed by a small amount at $t = 0$, and the gas its assumed perfect (Appendix C2 of Moody (1990)). The solution can be obtained by perturbation methods assuming that at order 0 the solution is the undisturbed state, i.e., $X^{(0)} = X_{eq}$, so it may be written:

$$X(t)=X^{(0)}+\varepsilon X^{(1)}(t)+\varepsilon^2X^{(2)}(t)+\ldots \tag{79}$$

The penetration length $X_{eq}$is in equilibrium when the jet pressure $P_s$is equal to the ambient valueP_∞, it is assumed that the process is polytropic and at equilibrium the jet volume is $V = V_{eq}$. Therefore, if the jet is not at equilibrium, it can be written:

$$P_s=P_\infty\left(\frac{V_{eq}}{V}\right)^n \tag{80}$$

Where n is the polytropic coefficient that depends on the type of polytropic process and is in the range $1 \le n \le 1.3$.

If there is a bubble which is expanding its radius $R = X$, then the volume change as $V\propto X^3$. But, if it is considered a cylinder with constant diameter d which is expanding its length X, then its volume change as $V\propto X$. For this reason, it is denoted by ν the dependence of the volume with the penetration length equal to $\nu = 3$ for a bubble, and $\nu = 1$ for a cylinder, or intermediate values for other geometries. Therefore, on account of these comments, it may be written:

$$P_s=P_\infty\left(\frac{X_{eq}}{X}\right)^{\nu n} \tag{81}$$

Therefore, the pressure in equation (81) can be expanded up to first order in the perturbation parameter as follows:

$$P_s=P_\infty\left(\frac{X_{eq}}{X}\right)^{\nu n}=P_\infty\left(\frac{X_{eq}}{X_{eq}+\varepsilon X^{(1)}(t)+o(\varepsilon^2)}\right)^{\nu n}=P_\infty\left(\frac{1}{\left(1+\varepsilon\frac{X^{(1)}(t)}{X_{eq}}+o(\varepsilon^2)\right)}\right)^{\nu n}$$
$$\cong P_\infty\left(1-\varepsilon\nu n\frac{X^{(1)}(t)}{X_{eq}}\right) \tag{82}$$

Where, as it is common practice $o(\varepsilon^2)$ means that terms of order ε^2 or higher are included in this term, and therefore this term is neglectable compared with the others.

Performing the expansion (79) in equation (78) and because of equation (82), and retaining only first order terms of the order parameter ε, yields the following equation for the amplitude of the oscillations:

$$\frac{d^2X^{(1)}(t)}{dt^2}+\frac{P_\infty}{\rho_l}\left(\frac{k_2}{k_1}\right)^2\frac{\nu n}{X_{eq}^2\left(1+\frac{8\alpha_E}{\cos\beta\,k_2^2}+\frac{1}{2}\left(\frac{8\alpha_E}{\cos\beta\,k_2^2}\right)^2\right)}X^{(1)}(t)=0 \tag{83}$$

Equation (83) can be rearranged and has the typical form of an oscillator:

$$\frac{d^2X^{(1)}(t)}{dt^2}+\omega_{oscil}^2X^{(1)}(t)=0 \tag{84}$$

with frequency given by:

$$f_{oscil}(Hz)=\frac{\omega_{oscil}}{2\pi}=\frac{k_2}{k_1}\frac{1}{2\pi}\sqrt{\frac{P_\infty}{\rho_l}\nu n\frac{1}{X_{eq}^2\left(1+\frac{8\alpha_E}{\cos\beta\,k_2^2}+\frac{1}{2}\left(\frac{8\alpha_E}{\cos\beta\,k_2^2}\right)^2\right)}} \tag{85}$$

It is observed that if in equation (85) the entrainment coefficient is set equal to zero, i.e., $\alpha_E = 0$, then equation (85) reduces to the Hong et al. equation for the frequency of the oscillations of a jet with penetration length X_{eq}.

3.3.2. Model with different expansion coefficients in the steam and liquid regions

Another approach that yields slightly different results is to consider that the diameter $d_1(x)$of the steam dominated region including the mixing region, and the diameter of the liquid dominated region denoted by $d_2(x)$, are given by the equations:

$$d_1(x)=d_0+2k_1'x=d_0+K_1x\;for\;0\le x\le X \tag{86}$$

$$d_2(x)=d_0+K_1X+2k_2'(x-X)=d_0+K_1X+K_2(x-X)\;for\;x\ge X \tag{87}$$

Where the expansion coefficients k_1' and k_2' are given by:

$$k_1'=tang\;\alpha \text{ and } k_2'=tang\;\beta \tag{88}$$

Being α and β the expansion angles of the steam-mixing region and liquid respectively, as displayed at Fig. 12.

In this case, the work performed by the steam against the liquid as the steam expands is given by:

$$Work_{sl}=(P_s-P_\infty)\int_0^X\frac{\pi}{4}(d_0+K_1x)^2dx=$$
$$(P_s-P_\infty)\frac{\pi}{4}X\left(d_0^2+d_0K_1X^2+\frac{1}{3}K_1^2X^3\right) \tag{89}$$

Also, equation (68) needs to be solved in this case, so using the previously explained perturbation method, the zero-order solution for the liquid velocity is:

$$u_l^{(0)}(x)=\frac{A(X)}{A(x)}\frac{dX}{dt}=\frac{(d_0+K_1X)^2}{(d_0+K_1X+K_2(x-X))^2}\frac{dX}{dt} \tag{90}$$

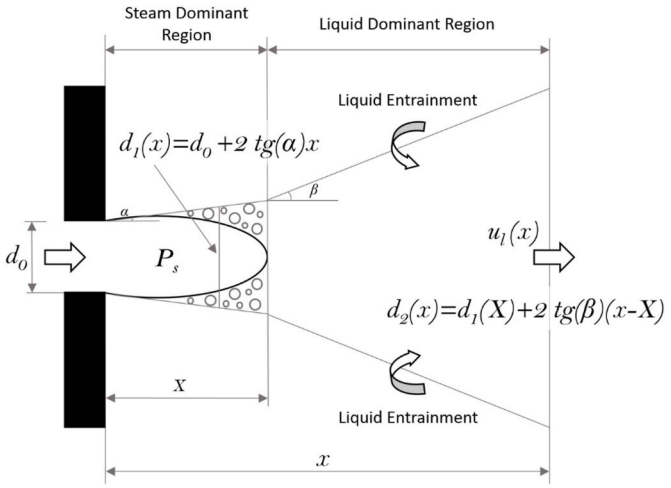

Fig. 12. Modelling of steam discharge into quiescent pool and jet expansion behavior.

The first order term of the liquid velocity is given by:

$$u_l^{(1)}(x) = \frac{1}{A(x)}\frac{\pi\alpha_E}{\cos\beta}\int_X^x d_2(x')u_l^{(0)}(x')dx' = \frac{A(X)}{A(x)}\frac{dX}{dt}\frac{4\alpha_E}{\cos\beta\, K_2}log\left(1+\frac{K_2(x-X)}{d_0+K_1X}\right) \quad (91)$$

After some calculus and simplifications, it is obtained the following result for the first order approximation of the velocity:

$$u_l(x) = \frac{A(X)}{A(x)}\frac{dX}{dt}\left(1+\frac{4\alpha_E}{\cos\beta\, K_2}log\left(1+\frac{K_2(x-X)}{d_0+K_1X}\right)\right) \quad (92)$$

Substituting the liquid velocity into the kinetic energy expression for the jet liquid region it is obtained after some calculus:

$$KE_l = \int_X^\infty \frac{1}{2}\rho_l u_l^2(x)A(x)dx = \frac{\pi}{8}\rho_l\frac{(d_0+K_1X)^3}{K_2}\left(\frac{dX}{dt}\right)^2\left(1+\frac{8\alpha_E}{\cos\beta\, K_2}+\frac{1}{2}\left(\frac{8\alpha_E}{\cos\beta\, K_2}\right)^2\right) \quad (93)$$

Equating equations (89) and (93), i.e., if the work performed by the steam against the liquid is given to the liquid region. Followed by derivation of the resulting equation with respect to the time yields after simplifications the following result:

$$\left(X+\frac{d_0}{K_1}\right)\frac{d^2X}{dt^2}+\frac{3}{2}\left(\frac{dX}{dt}\right)^2-\frac{1}{\rho_l}\left(\frac{K_2}{K_1}\right)\frac{(P_s-P_\infty)}{\left(1+\frac{8\alpha_E}{\cos\beta\, K_2}+\frac{1}{2}\left(\frac{8\alpha_E}{\cos\beta\, K_2}\right)^2\right)}=0 \quad (94)$$

Equation (94) is the jet dynamics equation when entrainment in the liquid region is considered, and it is assumed that the jet expands in the steam dominated region with angle α and in the LDR with angle β. This equation matches the Rayleigh-Plesset equation (Plesset, 1949) for the dynamics of a bubble when $d_0 = 0$, $K_1 = K_2$ and $\alpha_E = 0$. The new factors and corrections consider that the jet expand from a source of diameter d_0, and there is entrainment in the liquid region and that the volume expansion in both regions LDR and SDR is different.

Next, equation (94) is solved as in appendix C of Moody's book (1990), performing a perturbation expansion of the solution as in equation (79), with the initial conditions $X^{(0)}(0) = X_{eq}$ and $\dot{X}^{(0)}(0) = 0$. In addition, it is considered that the steam pressure evolution with time is governed by equation (82). Therefore, the equation obeyed by the time dependent part $X^{(1)}(t)$ is given in first order perturbation theory by:

$$\frac{d^2X^{(1)}(t)}{dt^2}+\frac{P_\infty}{\rho_l}\left(\frac{K_2}{K_1}\right)\frac{\nu\, n}{X_{eq}\left(X_{eq}+\frac{d_0}{K_1}\right)\left(1+\frac{8\alpha_E}{\cos\beta\, K_2}+\frac{1}{2}\left(\frac{8\alpha_E}{\cos\beta\, K_2}\right)^2\right)}X^{(1)}(t)=0 \quad (95)$$

Equation (95) is the equation of an oscillator as in equation (84) with frequency given by:

$$f_{oscil}(Hz) = \frac{\omega_{oscil}}{2\pi} = \frac{1}{2\pi}\sqrt{\frac{K_2}{K_1}\frac{P_\infty}{\rho_l}\nu n\frac{1}{X_{eq}\left(X_{eq}+\frac{d_0}{K_1}\right)\left(1+\frac{8\alpha_E}{\cos\beta\, K_2}+\frac{1}{2}\left(\frac{8\alpha_E}{\cos\beta\, K_2}\right)^2\right)}} \quad (96)$$

With $K_1 = 2\ tg\ \alpha$ and $K_2 = 2\ tg\ \beta$.

3.3.3. Model with momentum transfer to the liquid by condensation

In this model, it is assumed that the jet expands with an angle βin the liquid dominated region that entrains water from the surrounding, also it is assumed that a part of the kinetic energy of the steam jet is transferred to the liquid by the transfer of momentum by condensation that occurs before all the steam condenses completely. In this case the mechanical energy conservation equation is written as follows:

$$Work_{sl} + KE_{\substack{momentum\\ transf\ by\ cond}} = KE_l \quad (97)$$

Where, as in the previous sections $Work_{sl}$ is the expansion work performed by the steam against the liquid, KE_l is the kinetic energy that has the liquid in the liquid dominated region, and finally $KE_{\substack{momentum\\ transf\ by\ cond}}$ is the kinetic energy transferred from the steam to the liquid by condensation because as the steam condenses, the momentum is transferred from one phase to the other.

In this model, the work performed by the steam against the liquid if the steam jet expansion has the form of a hemi-ellipsoid, as shown in Fig. 13, is given by:

$$Work_{sl} = \int_{x=0}^{X}(P_s-P_\infty)\,\pi r(x)^2dx = \frac{\pi}{6}d_0^2\,X(P_s-P_\infty) \quad (98)$$

where to compute the integral of equation (98) it has been assumed, according to Fig. 13 and equation (18), that:

$$r(x) = \frac{d_0}{2}\sqrt{1-\frac{x^2}{X^2}} \quad (99)$$

The kinetic energy of the liquid KE_l in the liquid dominated region when entrainment is considered is obtained from equation (93) setting $K_1 = 0$, which yields:

$$KE_l = \int_X^\infty \frac{1}{2}\rho_l u_l^2(x)A(x)dx = \frac{\pi}{8}\rho_l\frac{(d_0)^3}{K_2}\left(\frac{dX}{dt}\right)^2\left(1+\frac{8\alpha_E}{\cos\beta\, K_2}+\frac{1}{2}\left(\frac{8\alpha_E}{\cos\beta\, K_2}\right)^2\right) \quad (100)$$

Considering that $K_2 = 2\ tang\beta$ and simplifying finally, KE_l can be expressed as follows:

$$KE_l = \frac{\pi}{8}\rho_l\frac{(d_0)^3}{K_2}\left(\frac{dX}{dt}\right)^2\left(1+\frac{4\alpha_E}{\sin\beta}+\frac{1}{2}\left(\frac{4\alpha_E}{\sin\beta}\right)^2\right) \quad (101)$$

It remains to calculate the amount of kinetic energy transferred to the liquid during the condensation because the steam that condenses into the liquid phase conserves its momentum. The kinetic energy contained in the liquid for $x \le X$, before all the steam condenses and which is due to the momentum transfer by condensation is a part of the liquid kinetic energy contained in this region. It is assumed that this amount is a fraction f_{mc} of the liquid kinetic energy in this region ($x \le X$), so it can be written:

$$KE_{\substack{momentum\\ transf\ by\ cond}} = \int_{fX}^{X} f_{mc}\frac{1}{2}\rho_l u_l^2(x)A_l(x)dx \quad (102)$$

Near the vent exit there is a small region where not condensation takes place, and the steam is superheated, then it is assumed that this region is a fraction f of the jet penetration length. The area of the liquid for $x \le X$, is:

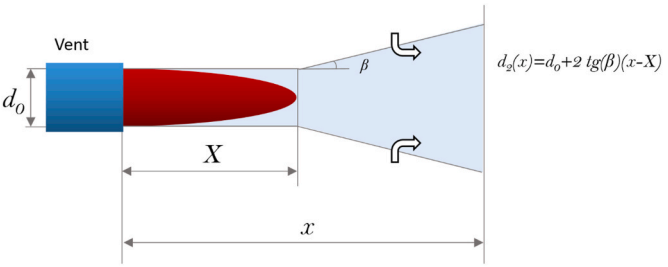

Fig. 13. Steam jet with prolate hemi-ellipsoidal shape condensing in water.

$$A_l(x) = \pi\left(r_0^2 - r(x)^2\right) = \pi r_0^2 \frac{x^2}{X^2} \tag{103}$$

The mass conservation equation of the liquid in the region ($x \leq X$) displayed in blue at Fig. 13 is given by the equation:

$$\frac{\partial}{\partial x}\left(\rho_l A(x) u_l(x)\right) = \pi \alpha_E d_0\, u_l(x) + 2\pi r(x)\sqrt{1 + (r'(x))^2}\,\frac{h\Delta T}{h_{fg}} \tag{104}$$

In a zero-order approximation, $u_l(x)$ can be computed from $u_l(X) = \frac{dX}{dt}$, using the continuity equation and neglecting the entrainment term and the condensation term in the right-hand side. So, the velocity $u_l(x)$ is given by:

$$u_l(x) = \frac{dX}{dt}\frac{A_l(X)}{A_l(x)} \tag{105}$$

Substituting equation (105) in equation (102), it is obtained

$$KE_{\substack{momentum \\ transf\ by\ cond}} = \frac{1}{2}\rho_l f_{mc}\int_{fX}^{X} u_l^2(x) A_l(x)dx = f_{mc}\frac{1-f}{f}\frac{\pi}{8}\rho_l d_0^2 X\left(\frac{dX}{dt}\right)^2 \tag{106}$$

So finally, equation (106) can be written in the form:

$$KE_{\substack{momentum \\ transf\ by\ cond}} = f_{mf}\frac{\pi}{8}\rho_l d_0^2 X\left(\frac{dX}{dt}\right)^2 \tag{107}$$

Where f_{mf} is a model parameter that will be obtained by fitting and from physical reasons.

Therefore, substituting the expressions for KE_l, $KE_{\substack{momentum \\ transf\ by\ cond}}$, and $Work_{sl}$, into the mechanical energy conservation equation (97), which is an extension of the mechanical conservation equation used by Hong et al. (2012), including the term $KE_{\substack{momentum \\ transf\ by\ cond}}$, and the entrainment in the liquid region, it is obtained:

$$\frac{\pi}{6}d_0^2 X(P_s - P_\infty) + f_{mf}\frac{\pi}{8}\rho_l d_0^2 X\left(\frac{dX}{dt}\right)^2 = \frac{\pi}{8}\rho_l \frac{(d_0)^3}{K_2}\left(\frac{dX}{dt}\right)^2\left(1 + \frac{4\alpha_E}{sin\,\beta} + \frac{1}{2}\left(\frac{4\alpha_E}{sin\,\beta}\right)^2\right) \tag{108}$$

Simplifying equation (108) yields:

$$\frac{d_0}{K_2}\left(1 + \frac{4\alpha_E}{sin\,\beta} + \frac{1}{2}\left(\frac{4\alpha_E}{sin\,\beta}\right)^2\right)\left(\frac{dX}{dt}\right)^2 - f_{mf}X\left(\frac{dX}{dt}\right)^2 = \frac{4X(P_s - P_\infty)}{3\rho_l} \tag{109}$$

Derivation of the previous equation with respect to the time gives after some simplifications the following result:

$$\left[\frac{d_0}{K_2}\left(1 + \frac{4\alpha_E}{sin\,\beta} + \frac{1}{2}\left(\frac{4\alpha_E}{sin\,\beta}\right)^2\right) - f_{mf}X\right]\frac{d^2X}{dt^2} + \frac{f_{mf}}{2}\left(\frac{dX}{dt}\right)^2 = \frac{2}{3}\frac{P_s - P_\infty}{\rho_l} \tag{110}$$

Equation (110) is the jet dynamics equation when entrainment in the liquid region is considered, and it is assumed that the steam jet has the shape of a prolate hemi-ellipsoid as displayed at Fig. 13, and in addition the liquid expands by entrainment in the LDR with angle β. Also, it is considered the kinetic energy received by the liquid from the momentum conservation of the condensed steam.

Next, equation (110) is solved as in appendix C of Moody's book (1990), performing a perturbation expansion of the solution as in equation (79), with the initial conditions $X^{(0)}(0) = X_{eq}$ and $\dot{X}^{(0)}(0) = 0$. In addition, it is considered that the steam pressure evolution with time is governed by equation (82). Therefore, the equation obeyed by the time dependent part $X^{(1)}(t)$ is given in first order perturbation theory by:

$$\frac{d^2X^{(1)}}{dt^2} + \frac{2}{3}\frac{P_\infty \nu\, n}{\rho_l}\frac{1}{X_{eq}\left[\frac{d_0}{K_2}\left(1 + \frac{4\alpha_E}{sin\,\beta} + \frac{1}{2}\left(\frac{4\alpha_E}{sin\,\beta}\right)^2\right) - f_{mf}X_{eq}\right]}X^{(1)} = 0 \tag{111}$$

Equation (111) is the equation of an oscillator as in equation (84) and (95) with frequency given by:

$$f_{oscill}(Hz) = \frac{1}{2\pi}\sqrt{\frac{2}{3}\frac{P_\infty \nu\, n}{\rho_l}\frac{1}{X_{eq}\left[\frac{d_0}{K_2}\left(1 + \frac{4\alpha_E}{sin\,\beta} + \frac{1}{2}\left(\frac{4\alpha_E}{sin\,\beta}\right)^2\right) - f_{mf}X_{eq}\right]}} \tag{112}$$

Good results are obtained for all cases taking $f_{mf}X_{eq}$ to be of the order of the exit vent diameter with a correction that considers the pool temperature as will be discussed in the next section.

3.4. Model results, comparison with experimental data and discussion for the SC and IOC map regions

The purpose of this section is to compare the results of the previous formulas with the experimental data of Hong et al. (2012). Hong et al. measurements were performed for steam mass flux values ranging from 200kg/m^2s to 900 kg/m^2s, and pool temperatures ranging from 35 °C to 95 °C. According to the map of Cho et al. (1998), displayed at Fig. 2, the measurements with low mass fluxes, approximately between 200 and 300 kg/m^2s are at the condensation oscillation regime (CO). However, when the mass flux increased maintaining the pool temperature constant there is a change of regime from the CO regime, when all the jet interface oscillates violently, to the stable condensation regime SC, when only the oscillation at the end of the jet interface is important. Obviously, as it is observed in Fig. 2, the transition regime from CO to SC takes place at higher mass fluxes when the pool temperature increases. Finally, it is also observed in Fig. 2 that for pool temperatures above 85 °C there are two additional changes of regime: to bubbling condensation oscillation (BCO) for steam mass fluxes below 350 kg/m^2s and to interfacial condensation oscillations (IOC) for steam mass fluxes above 350 kg/m^2s.

There is a set of parameters values that must be discussed before we compare the results with the experimental data. The first one is the angle of expansion in the liquid dominated region β, angle which is around 30°

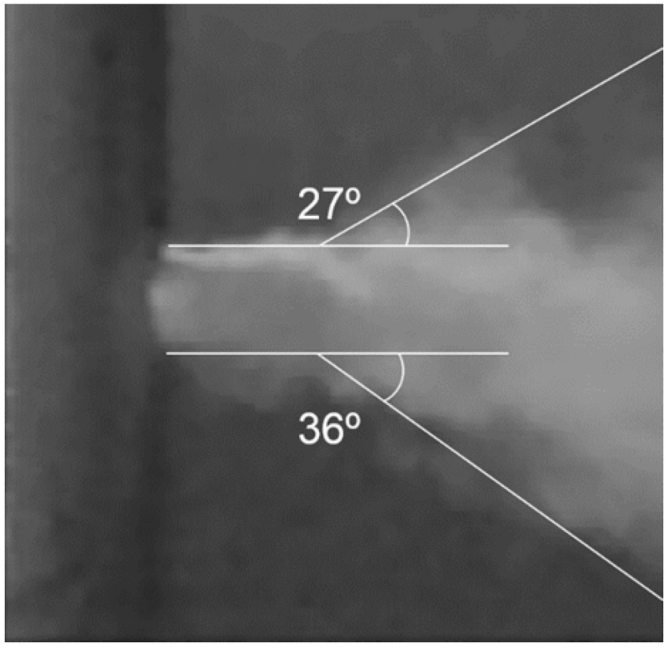

Fig. 14. Expansion angles in the upper and lower parts of the jet in the liquid dominated region. The photographs obtained with a high-speed camera are from Hong et al. paper (2012).

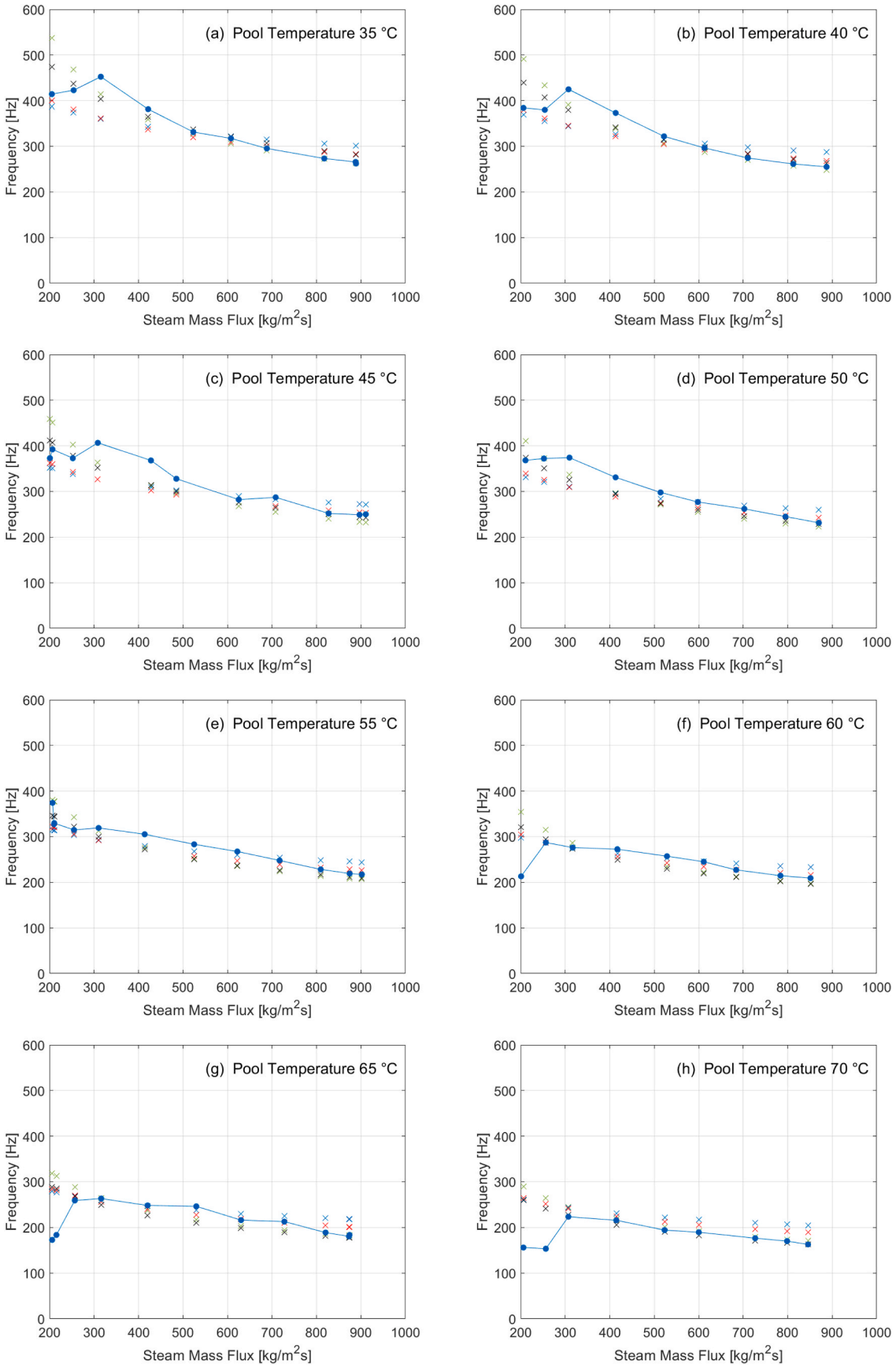

Fig. 15. Comparison of the predicted frequencies using equation (114) with the experimental ones measured by Hong et al. (2012) using four different correlations for the penetration length.

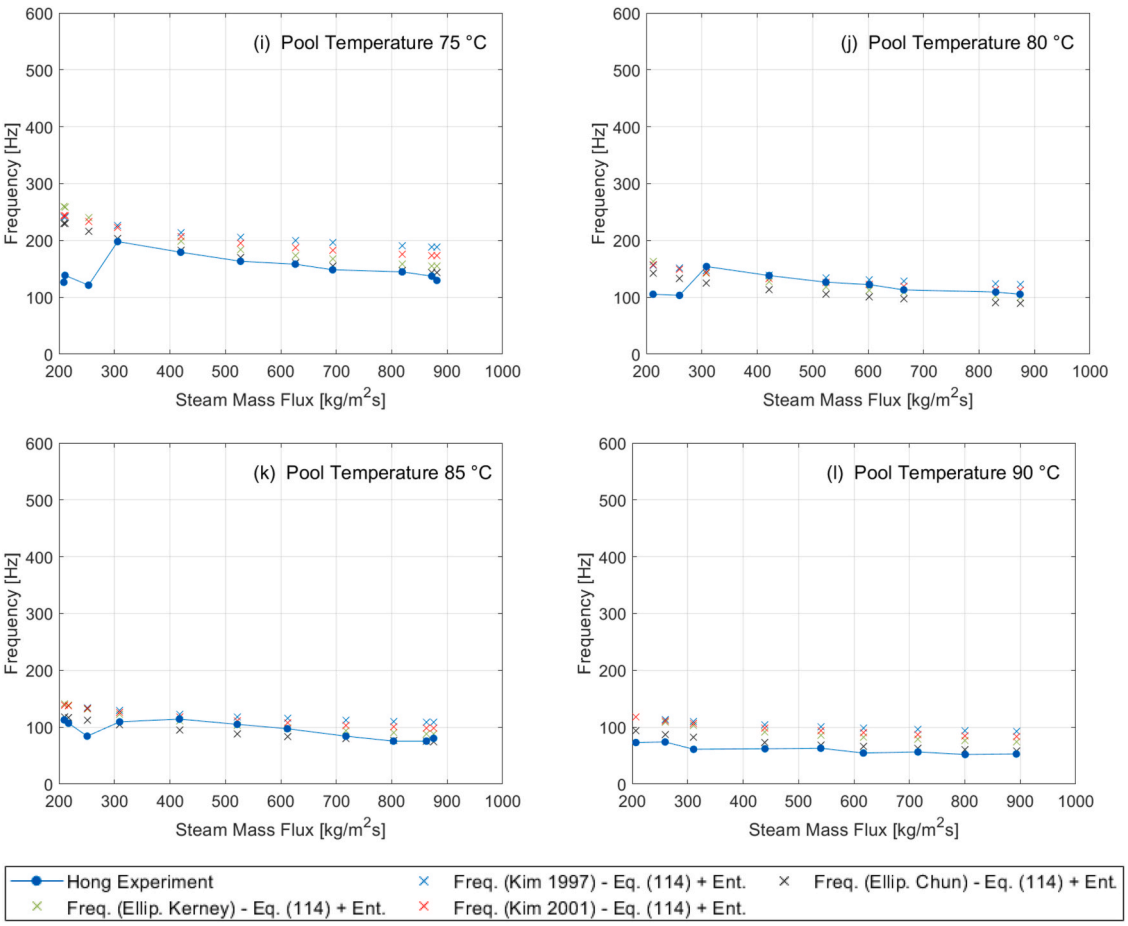

Fig. 15. (*continued*).

(Fig. 14). The images have been taken from the paper of Hong et al. (2012). Obviously, the β values depend on the mass flux injected, the subcooling temperature of the pool, the vent diameter and so on. Another problem is that the measured expansion angle is a slightly bigger in the lower part of the jet than in its upper part, so an average angle of 33° has been taken for the model.

The parameter value used for the polytropic coefficient has been taken equal to $n = 1.3$. Another important parameter is the volume expansion with the characteristic length. For a bubble the value of this parameter is $\nu = 3$, this means that the volume change with the bubble radius as $V \sim R^3$, however if the shape of the steam jet is a cylinder of constant radius, then $V = \pi r_0^2 X \sim X$, in this case $\nu = 1$. Then, this parameter varies between $1 \leq \nu \leq 3$. In this case, the volume variation of the jet steam is not exactly like a constant cylinder expansion but has a small expansion in the other two dimensions, so finally $\nu = 1.3$ has been taken.

For the entrainment coefficient α_E of jets Papanicolaou and List (1988) measured its value and obtained $\alpha_{E,jet} = 0.055$, also Rodi (1982) proposes to use $\alpha_{E,jet} = 0.052$. Other authors as Carazzo et al. (2006) give higher values for this coefficient ranging in the interval $0.065 < \alpha_{E,jet} < 0.084$. More recently Van Reeuwijk et al. (2016) obtained the entrainment coefficient by simulation with DNS, for jets they obtained the value of $\alpha_{E,jet} = 0.067$. This model uses the value of $\alpha_{E,jet} = 0.0595$, which is compatible with most experimental data. For the parameter K_2, its value is computed from $K_2 = 2 \tan \beta$, as defined in equations (87) and (88). The average penetration length l_p of the steam in the subcooled pool was computed with four different correlations explained previously in section 2, Kerney-Ellipsoidal, Chun-Ellipsoidal and two of Kim, as displayed at Table 2. Therefore, in equations (96) and (112), X_{eq} is the jet penetration length, $X_{eq} = l_p$.

Finally, to compute $f_{mf} X_{eq}$ that is related to the initial jet length, where no condensation takes place, note that this distance is of the order of the vent diameter and that changes slightly with the pool temperature T. So, it is used:

$$f_{mf} X_{eq} \approx (f_E - f_T (T - T_0)) d_0 \tag{113}$$

Where $f_E = 1$, $f_T = 0.001$,$T_0 = 60^{\circ}C$, and T is the pool temperature in centigrade degrees and T_0 a reference temperature. So, to compare the predicted frequency with the experimental data of Hong et al. (2012), the following expressions are used:

$$f_{oscill}(Hz) = \frac{1}{2\pi} \sqrt{\frac{2}{3} \frac{P_\infty \nu\, n}{\rho_l} \frac{1}{X_{eq} \left[\frac{d_0}{K_2} \left(1 + \frac{4\alpha_E}{\sin \beta} + \frac{1}{2} \left(\frac{4\alpha_E}{\sin \beta} \right)^2 \right) - (f_E - f_T (T - T_0)) d_0 \right]}} \tag{114}$$

And neglecting the entrainment and pool temperature effects on the previous equation, it reduces to:

$$f_{oscill}(Hz) = \frac{1}{2\pi} \sqrt{\frac{2}{3} \frac{P_\infty \nu\, n}{\rho_l} \frac{1}{X_{eq} \left[\frac{d_0}{K_2} - f_{NE} d_0 \right]}} \tag{115}$$

Where the fitting constant in equation (115) has been taken as constant, $f_{NE} = 0.62$. Fig. 15 display the experimental data obtained by Hong et al. (2012) for the frequency of the oscillations versus the mass flux at different pool temperatures. Also, these same figures display the frequencies of the oscillations computed with equation (114) for different mass fluxes and pool temperatures and different correlations for the

penetration length l_p of the steam in water. The correlations used to predict the value of the parameter $X_{eq} = l_p$ in equation (114) were the four ones mentioned above, Ellipsoidal-Kerney, Ellipsoidal-Chun, Kim et al. (1997), Kim et al. (2001). The values used in equation (114) for the parameters were $f_E = 1$, $f_T = 0.001$, $T_0 = 60°C$ and in equation (115) $f_{NE} = 0.062$. The value of angle $\beta = 34°$ and the parameter $K_2 = 2 \tan \beta$. The polytropic coefficient was set to $n = 1.3$, and the parameter $\nu = 1.3$. The predictions of equation (114) are in general better than the predictions given by equation (115), especially for higher pool temperatures above 80 °C. Also, it is necessary to point out that equation (114) predicts the frequencies well even at 80 °C and 85 °C. Now according to Fig. 2, for mass fluxes around $210\ kg/m^2s$ there is a change of regime from CO to SC at a pool temperature of 20 °C. This transition regime limit G_{lim} for the mass flux increases with the pool temperature and is equal to $300 kg/m^2s$ at 60 °C. In Fig. 15, it is observed that in general equation (114) considering the entrainment and the pool temperature effects predicts very well the frequency for all the pool temperatures. The cases for the highest pool temperature 95 °C are not displayed, because considering the map of Fig. 2, this case is at the limit of another transition regime and will not be studied here, because of it is necessary to consider the changes that produces the regime transition on the frequency formula.

It is observed at Fig. 16 (a) and 16 (b) that the ellipsoidal Kerney and the ellipsoidal Chun correlations give good prediction results for all the pool temperatures between 35 °C and 75 °C and all the mass fluxes ranging from 300 to 900 kg/m^{2}s. As observed in the plot of predicted versus experimental values of the frequency, Fig. 16, all the results lie inside the band $\pm 15\%$. In addition, when using Kim et al. (1997 and 2001) correlations for estimating the penetration length in the frequency formula the results, displayed at Fig. 16 (c) and (16 (d), are a little bit worse, as some points are above the +15% error band although close to this band, and a few points are below the −15% band of error, but also close to this band. Also notice that the quality of the results obtained for the predicted frequencies as displayed in Fig. 16-a, 16-b, 16-c, and 16-d follows the same order than the RMSE obtained for the predicted steam penetration length as shown in Table 2.

Let us compare now the results obtained with Hong et al. (2012) model with the results obtained with Hong's model when the entrainment is included in the liquid dominated region. In this case, the model results of Hong et al. (2012) are given by equation (85) setting the entrainment parameter equal to zero i.e., $\alpha_E = 0$. For Hong et al. model considering entrainment, $\alpha_E = 0.059$ is selected. The values of the rest of coefficients where fixed to the following values: the ratio $k_2/k_1 = 3.72$, the polytropic coefficient $n = 1.3$, the exponent for the expansion of the volume in terms of the radial distance was set to $\nu = 3$, as in Hong's paper. For the entrainment case, the value of the coefficient k_2 is needed, we set $k_2 = 1.6$, so $k_1 = 0.43$, which yields $k_2/k_1 = 3.72$. The chosen value of the angle was $\beta = 33°$, this angle appears in the frequency formula, expression that includes the entrainment because the entrainment area in the liquid region depends on β. Fig. 17 show the comparison of the predicted results using equation (85) when entrainment is considered, $\alpha_E = 0.059$, and when entrainment is neglected, $\alpha_E = 0$, in this last case one gets the equation previously obtained by Hong et al. (2012).

It is observed that, in general, the prediction performed considering the entrainment in the LDR zone yields frequency predictions that are lower than the predictions with $\alpha_E = 0$ because of the inertial mass opposed to the interface oscillations is bigger when entrainment is

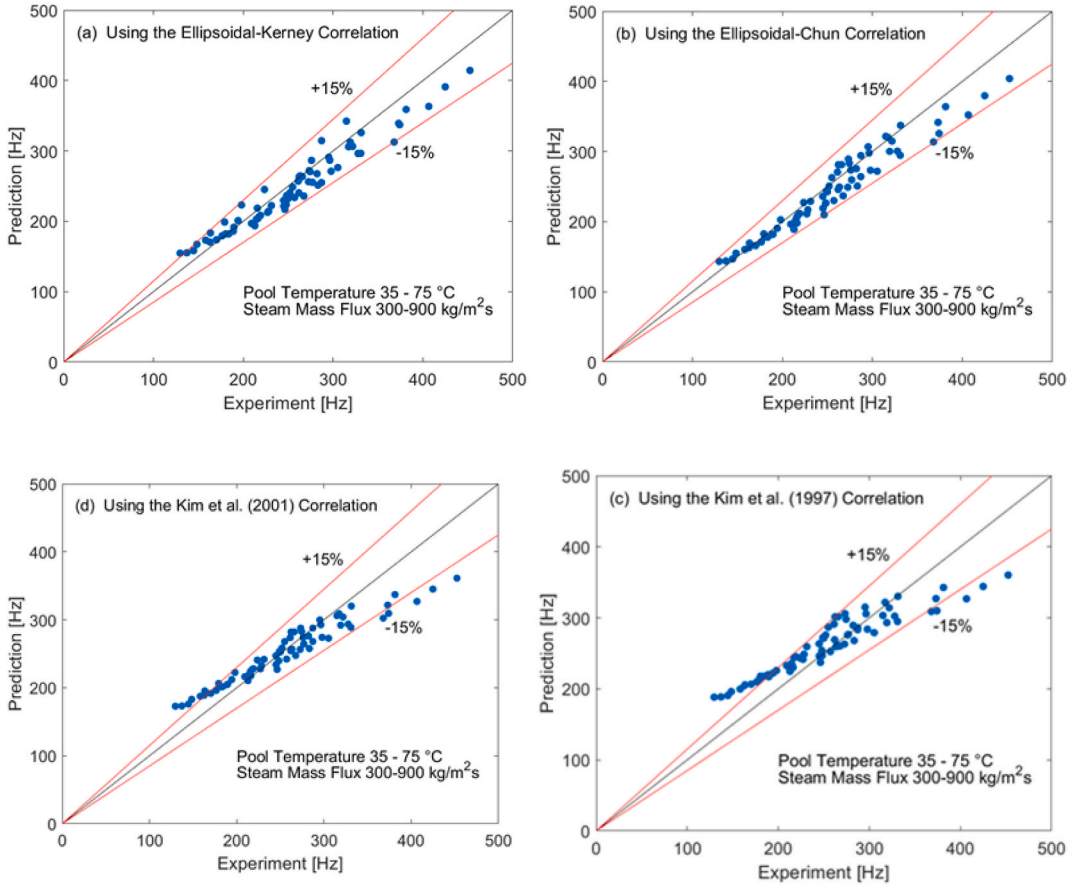

Fig. 16. Experimental frequencies versus predicted ones obtained with equation (114) considering entrainment for pool temperatures ranging from 35 °C to 75 °C and mass fluxes from 300 to 900 kg/m^{2}s. The steam penetration length was obtained with a) Ellipsoidal-Kerney correlation, (b)Ellipsoidal-Chun correlation, (c) Kim et al. (1997) correlation, (d) Kim et al. (2001) correlation.

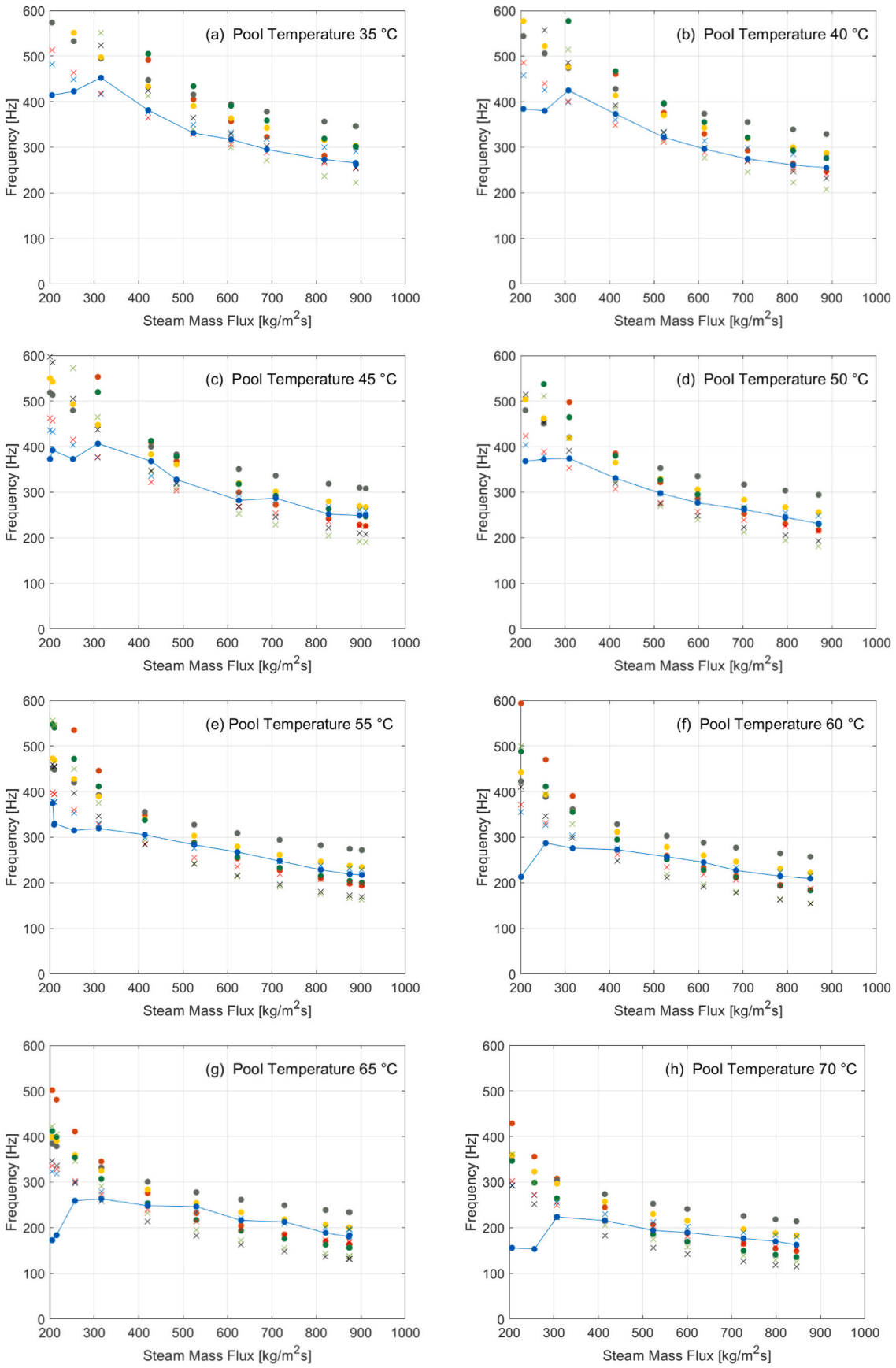

Fig. 17. Comparison of the predicted frequencies using Hong equation with entrainment, equation (85) and without entrainment with the experimental data measured by Hong et al. (2012), using different correlations for the penetration length.

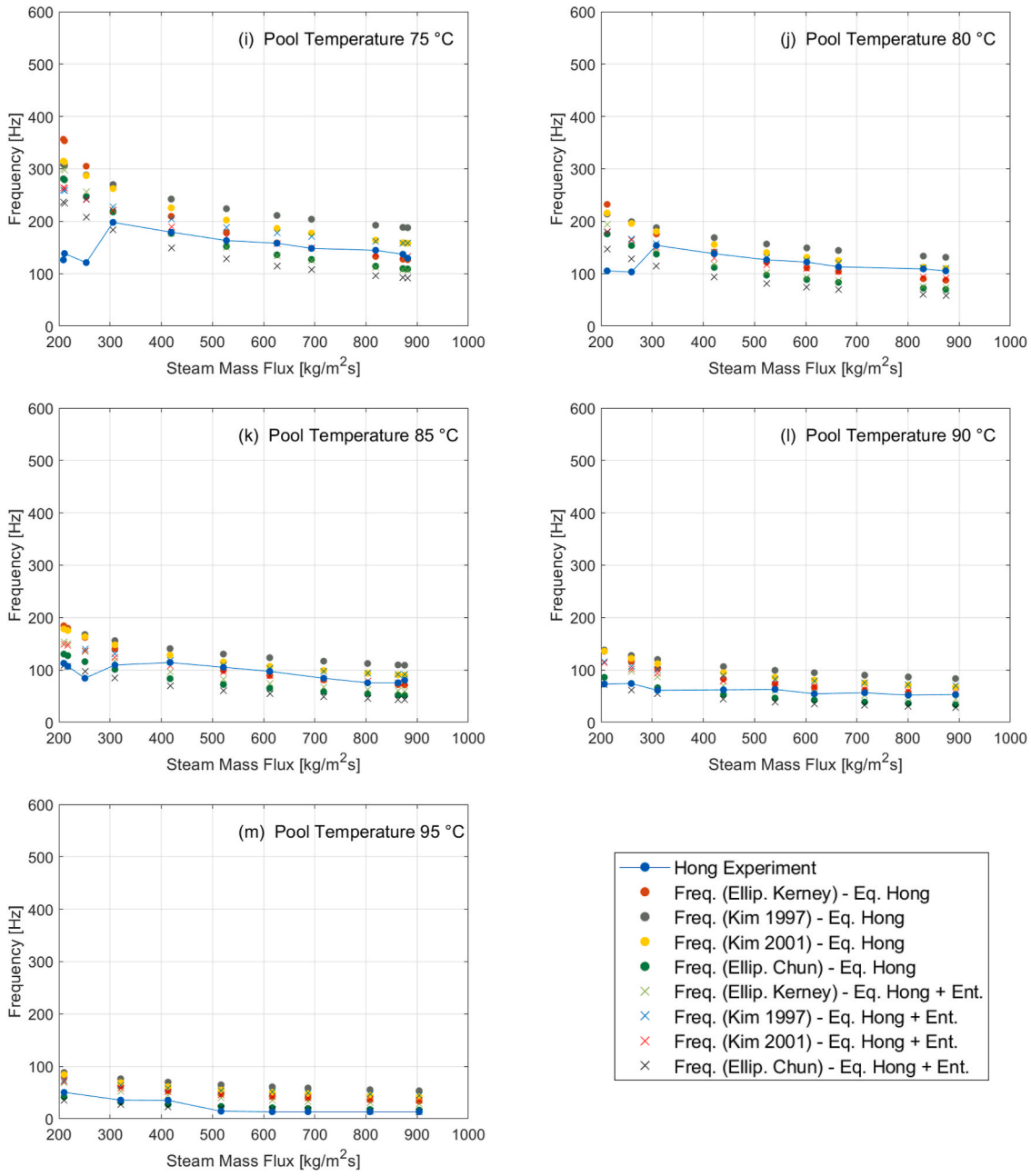

Fig. 17. (*continued*).

considered. Furthermore, it can be highlighted that the model considering the entrainment works well even at high temperatures of the pool as displayed at Fig. 17 (j), 17 (k), 17 (l) and 17 (m).

It is observed in Fig. 18 (a) and 18 (b) that when the Hong's formula with entrainment is used for the frequency, then the Kim et al. (2001) and the Kim et al. (1997) correlations for the penetration length give the best prediction results for all the pool temperatures between 35 °C and 75 °C and all the mass fluxes ranging from 300 to 900 kg/m^{2}s. As shown in Fig. 18, the plot of predicted versus experimental values of the frequency, all the results lie inside the band $\pm 15\%$. In addition, when using ellipsoidal-Kerney and ellipsoidal-Chun correlations for the penetration length in the frequency formula the results are slightly worse, since some points are above the +25% error band but close to this band, and a few points are below the −25% band of error but also close to this band.

Finally, taking as figure of merit the root mean-square relative error defined in the standard way:

$$RMSRE(f) = \sqrt{\frac{1}{N}\sum_{i=1}^{N}\left(\frac{f_{model,i} - f_{exp,i}}{f_{exp,i}}\right)^2} \tag{116}$$

Where N is the number of experimental points for temperatures from 35 °C to 75 °C and for the mass fluxes ranging from $300 kg/m^2 s$. Table 3 shows the RMSRE values obtained with the new equation (114), which includes entrainment and Hong's equation including entrainment. The smallest RMSRE value, as displayed at Table 4, was obtained using equation (114) plus entrainment, i.e., $\alpha_E \neq 0$ and the ellipsoidal-Chun correlation for the penetration length of the steam. If one uses equation (85) with entrainment, the smallest value was obtained with Kim et al. (2001) correlation for the penetration length. In general, the RMSRE values are smaller with equation (114) plus entrainment, as shown in Table 4.

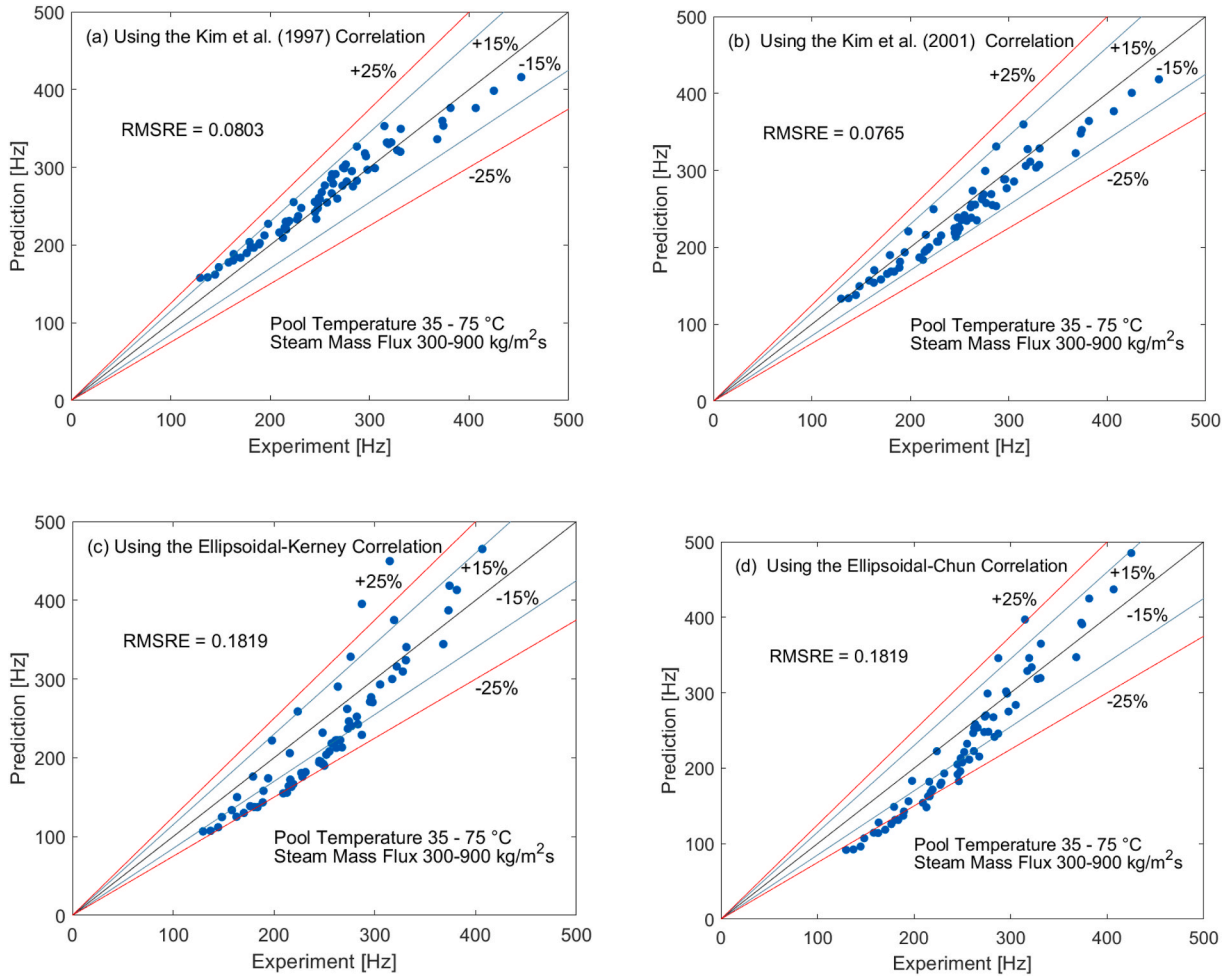

Fig. 18. Experimental frequencies versus predicted ones obtained with Hong equation considering entrainment (equation (85)) for pool temperatures ranging from 35 °C to 75 °C and mass fluxes from 300 to 900 kg/m^{2}s. The steam penetration length was obtained with: (a) Kim et al. (1997), (b) Kim et al. (2001), (c) Ellipsoidal-Kernel and (d) Ellipsoidal-Chun correlations.

Table 4
RMS relative error (RMSRE) calculated using equation (114) including entrainment (Ent.) and equation (85) including entrainment.

Correlation used to obtain l_p in the equation for $f_{oscillation}$	RMSRE (Eq. (114) + Ent.)	RMSRE (Eq. (85) Hong + Ent.)
Ellipsoidal-Kerney	0.0780	0.1819
Ellipsoidal-Chun	0.0681	0.1819
Kim-97	0.1466	0.0803
Kim-2001	0.1091	0.0765

4. Conclusions

In this paper we have reviewed and analyzed the instabilities that take place during the discharge of steam in subcooled water pools and tanks and produced by the direct contact condensation of steam (DCC) at the steam-water interface. Because an important parameter for these processes is the jet penetration length, first we have compared the correlations developed by authors as Kim et al. (1997), Kim et al. (2001), Kerney et al. (1972) displayed at Table 2 with Kerney et al. experimental data obtaining the root-mean-square-error. In addition, we have developed in equation (24) an alternative form to Kerney correlation valid for hemi-ellipsoidal prolate steam jets and a general expression in equation (27) for the penetration lengths of this type of jets. Because the jet penetration length, as shown in equation (24), depends on the transport modulus (Stanton number). Then, a new expression for this length it is deduced by substituting in equation (24) the transport modulus by the correlation obtained by Chun et al. (1996), being denoted this expression as the Ellipsoidal-Chun in Table 2. Also, we have obtained by a fitting procedure of equation (27) to Kerney experimental data using the MATLAB routine NLFIT the unknown coefficients, b_i, which yields a new correlation for the penetration length denoted as Ellipsoidal-Kerney. It is noteworthy to remark that this ellipsoidal-Kerney correlation has a root-mean-square-error smaller than the Kerney original correlation, as shown at Table 2.

Several types of instabilities produced by the local steam discharges through vents or nozzles have been reviewed in this paper. These local discharges can produce mainly six types of instabilities known as "Chugging" (C), "Transition to Condensation Oscillations" (TCO), "Condensation Oscillations" (CO), "Bubbling Condensation Oscillations" (BCO), "Stable Condensation" oscillations (SC), and "Interfacial Oscillation Condensation" (IOC). In section (3.1), we have reviewed the transition to condensation oscillations (TCO) and the condensation oscillations (CO) using a hemi-ellipsoidal model for the condensation of the steam jet based on previous works of Aya and Nariai (1986,1991) that used a cylindrical jet shape, Fukuda (1982) that used a spherical jet shape and Gallego-Marcos et al. (2019) that correct Fukuda and Saitoh. correlation for the condensation heat transfer coefficient considering only the detachment phase of the spherical bubble. In this paper we have considered a hemi-ellipsoidal prolate jet, that according to the high-speed photographs is more realistic for many cases. The determination of the temperature threshold for the stability of low and high

frequency oscillations is performed based on non-linear dynamics methods considering the Lyapunov exponents and the Hartman-Grobman theorem (Guckenheimer and Holmes 1986), (Muñoz-Cobo and Verdú 1991) that yields a clearer and modern methodology compared with previous ones (Fukuda 1982; Aya and Nariai 1991), although the results are similar. However, the method used in this paper permits to be extended in the future to obtain the limit cycle oscillation behavior when including the non-linear terms. Table 3 displays the subcooling temperature thresholds for low and high frequency oscillations in discharges of steam in subcooled pools for spherical, cylindrical, and hemi-ellipsoidal prolate jets extending previous development of Fukuda and Saitoh (1982) and Aya and Nariai (1986,1991).

Two types of comparisons have been performed in this paper considering the subcooled threshold for high and low frequency oscillations. First, we have compared the high frequency oscillations threshold with the experimental results of Aya and Nariai (1986) and Fukuda (1982) for low steam mass fluxes ranging from 0 to 30 $kg/\ m^2s$. The subcooled threshold temperature for high frequency oscillations was computed with the formula for a hemi-ellipsoidal prolate steam jet, displayed at Table 3, and the correlation of Gallego-Marcos et al. (2019) for the heat transfer coefficient to obtain the penetration length using equation (60). It is observed in Fig. 5 that the predicted subcooling threshold for the high frequency oscillations ΔT_{THf} versus the steam mass flux lies between the results measured by Fukuda and Saitoh (1982) and Aya and Nariai (1986,1991). An additional observation is that ΔT_{THf} computed solving equation (61) deduced considering equation (60) and the correlation of Gallego-Marcos et al. (2019) diminishes with the mass flux but not with a constant slope value as observed experimentally. If one uses Fukuda (1982) correlation for the heat transfer coefficient, the result is that the predicted subcooling threshold versus the steam mass flux for high frequency oscillations is constant and does not depend on the mass steam flux G_S.

We have found that the results for ΔT_{THf} are very sensitive to the polytropic coefficient value of the condensing steam jet. The polytropic coefficient value for this case should be close to 1.08 as discussed in section (3.1). Additionally, we have seen that for polytropic processes, where the steam suffers expansion and contractions the polytropic index should be in the interval $1.08 \leq n \leq 1.2$ (Soh and Karimi 1996, Romanelli et al., 2012). Therefore, it is recommended measurements of the polytropic coefficient at the conditions of this kind of experiments. For higher liquid temperatures bigger than 90 °C, the steam condensation diminishes when rising the pool temperature and the polytropic coefficient should be close to the value of 1.3 used for adiabatic processes.

Secondly, in section 3.2, we compared the liquid temperature threshold $T_{l,TLf} = T_{sat} - \Delta T_{TLf}$, for the occurrence of low frequency oscillations computed using equation (57) deduced in this paper, considering equation (60) for the penetration length and the correlation of Gallego-Marcos et al. (2019) to obtain the HTC, with the experimental data of Chan and Lee (1982). We have obtained that the predicted liquid temperature threshold versus the mass flux practically matches the experimental data for low mass fluxes. In this case, the results that are closer to the experimental ones are obtained with a polytropic coefficient of 1.3 as displayed at Figs. 7 and 9. This behavior is logic considering that the liquid temperature is higher than 90 °C and the exchange of heat at the interface diminishes as the process approaches to the conditions of an adiabatic process. The interesting result is that the slope of the curve of $T_{l,TLf}$ versus G_S also matches the slope of the experimental data, so the physics of the process is well captured in comparison with previous results (Arinobu, 1980; Fukuda and Saitoh, 1982). This threshold for the occurrence of low frequency oscillations corresponds in the map to the threshold for transition to bubbling condensation oscillations regime in Cho et al. (1998) and to the transition to ellipsoidal oscillatory bubble regime in Chan and Lee (1982), see Figs. 1 and 2.

Consequently, we decided to compare the liquid temperature threshold for low frequency oscillations with the experimental results of Chan and Lee (1982) and Cho et al. (1998), for a bigger interval of mass fluxes ranging from 0 to 200 kg/m^2s. The model results for $T_{l,TLf} = T_{sat} - \Delta T_{TLf}$, as shown at Fig. 10, match the experimental data of Chan and Lee for mass fluxes below 50 kg/m^2s and when the mass fluxes are above 50 kg/m^2s the predicted results tend progressively to the experimental data of Cho et al. (1998). So that for mass fluxes above 75 kg/m^2s, the predicted threshold temperatures match the experimental ones of Cho et al. (1998). Although, the temperature differences between predicted and experimental results are very small, it is necessary to perform more precise measurements to confirm the liquid temperature threshold for bubbling condensation oscillations (BCO).

Finally, in section (3.3), first we review in subsection (3.3.1) the Hong et al. model (2012) for modelling the oscillations in the stable condensation regime when only the final part of the jet oscillates. The next step was to add to the Hong et al. model the entrainment of the surrounded liquid in the liquid dominated region (LDR) not considered by Hong. Obviously if the amount of liquid that is entrained into the jet increases as occurs in this type of jets, then the inertial mass in the LDR region growths, which obviously diminishes the frequency of the oscillations. As observed in equation (85), the increment in the entrainment coefficient α_E tend to diminish the frequency of the oscillations as physically expected. Also, if the jet angle β increases then the frequency also diminishes, the reason is that the entrainment area becomes larger and therefore increases the mass of entrained liquid, which rises the inertial mass and therefore diminishes the oscillation frequency. It is observed in equation (85) that when the entrainment coefficient is set to zero the new formula reduces to Hong's original formula for the frequency of the oscillations. The Hong's model parameters considering the entrainment were adjusted to the experimental data of Hong et al. (2012). Then, it is observed that using the correlations of Kim et al. (1997 and 2001) for the jet penetration length all the data in the plot of experimental frequencies versus the predicted ones were inside the error band of $\pm 15\%$, as displayed at Fig. 18 (a) and 18 (b). While for the ellipsoidal-Kerney and ellipsoidal-Chun models, all the data were inside the $\pm 25\%$error band, as shown in Fig. 18 (c) and 18 (d). In both cases, we considered ranges of steam mass fluxes from 300 to 900 kg/m^2s and pool temperatures inside the interval 35 to 75 °C.

Then in section 3.3.2, we studied a generalization of Hong's model with different expansion coefficients in the steam and liquid dominated regions starting from an initial diameter d_0. This approach is equivalent to consider a steam jet expanding from a virtual origin located at $-x_v$ and radius $r(x) = k'_j(x + x_v)$, being $k'_j x_v = r_0$. This approach gives for the oscillation frequency the result provided by equation (96). However, many of the experimental observations for mass fluxes higher than $200 kg/m^2$s shows a hemi-ellipsoidal steam jet in the steam dominated region where the water close to the jet receives kinetic energy from the work performed by the steam during the expansion and the momentum transfer during the steam condensation. So, we have improved the balance of mechanical energy performed by Hong et al. (2012), adding to the mechanical work performed by the steam on the liquid during the jet expansion, the kinetic energy transferred to the liquid by the momentum transfer during the condensing process. As shown in equation (97), see section (3.3.3), these two contributions are equated to the kinetic energy in the liquid dominated region, where we have considered the entrainment of liquid from the surrounding ambient that produces a jet expansion with angle β that can be measured experimentally. In this approach, we have obtained after some simplifications equations (114) and (115) for the frequency, where equation (115) is a simplification of equation (114) neglecting the entrainment and the pool temperature effect on the noncondensing length near the vent. In this case, if we represent the predicted frequencies versus the experimental ones for all the mass fluxes ranging from 300 kg/m^{2}s to 900 kg/m^{2}s, and pool temperatures ranging from 35 °C to 75 °C, it is observed at Fig. 16 (a), 16 (b) that the model predictions with equation (114) are within the $\pm 15\%$ error bands, when we use the correlations of ellipsoidal-Chun and

ellipsoidal-Kerney to compute the jet penetration length in equation (114). However, if we use the correlations of Kim et al. (1997 and 2001) for l_p, then most of the points as displayed in Fig. 16 (c) and 16 (d) are inside the $\pm 15\%$ error bands and a few ones are a little above or below, but always close to the error bands. Also, the new frequency formula given by equation (114) yields in general smaller values for the RMSRE as shown in Table 4. So, the new improvements to the Hong model gives better results and diminish the discrepancies between predictions and experimental data. So more precise measurements of the expansion angles in the LDR and SDR regions are necessary to improve the model predictions.

Author contributions

J.L.Muñoz-Cobo: Conceptualization, Formal analysis, Data curation, Funding acquisition, Investigation, Methodology, Software, Supervision, Writing – original draft, **D.Blanco:** Data curation, Formal analysis, Investigation, Software, Validation, Writing – review & editing, **C.Berna:** Formal analysis, Methodology, Writing – review & editing, **Y. Córdova:** Methodology, Validation, Visualization, Writing – review & editing.

Declaration of competing interest

The authors declare the following financial interests/personal relationships which may be considered as potential competing interests: Yaisel Cordova reports financial support was provided by Valencia Directorate of Research Culture and Sport.

Data availability

Data will be made available on request.

Acknowledgments

One of the authors of this project received a Grisolía scholarship to perform his PhD. The authors of this paper are indebted to Generalitat Valenciana (Spain) by its support under the Grisolía scholarship program.

References

Aya, I., Nariai, H., 1986. Occurrence of pressure oscillations induced by steam condensation in pool water. Bull. JSME 29 (No. 253), 2131–2137.
Aya, I., Nariai, H., 1991. Elevation of heat transfer coefficient at direct contact condensation of cold water and steam. Nucl. Eng. Des. 131, 17–24.
Aya, I., Nariai, H., Kobayashi, M., 1980. Pressure and fluid oscillations in vent system due to steam condensation, (I) experimental results and analysis model for chugging (I). J. Nucl. Sci. Technol. 17 (7), 499–515. https://doi.org/10.1080/18811248.1980.9732617.
Arinobu, M., 1980. Studies on the dynamic phenomena caused by steam condensation in water. In: Proceedings of the First International Topical Meeting on Nuclear Reactor Thermal-Hydraulics, vol. 1. NUREG/CP-0014, Saratoga New York, pp. 293–302, 9-12.
Chan, C.K., Lee, C.K.B., 1982. A regime map for direct contact condensation. Int. J. Multiphas. Flow 8 (No. l), 11–20.
Carazzo, G., Kaminski, E., S. Tait, S., 2006. The route to self-similarity in turbulent jets and plumes. J. Fluid Mech. 547, 137.
Carey, V.P., 1992. Liquid-Vapor Phase-Change Phenomena, Series in Chemical and Mechanical Engineering Published. Hemisphere Publishing Corporation.
Chandra, A., Keblinski, P., 2020. Investigating the validity of Schrage relationships for water using molecular-dynamics simulations. J. Chem. Phys. 153, 124505 https://doi.org/10.1063/5.0018726.
Cho, S., Song, C.H., Park, C.K., Yang, S.K., Chung, M.K., 1998. Experimental study on dynamic pressure pulse in direct contact condensation of steam jets discharging into subcooled water. In: Proc. 1st Korea-Japan Symposium on Nuclear Thermal Hydraulics and Safety (NTHAS98), pp. 291–298. Pusan, Korea.
Chun, M.H., Kim, Y.S., Park, J.W., 1996. An investigation of direct condensation of steam jet in subcooled water. Int. Commun. Heat Mass Tran. 23 (7), 947–958.
Collier, J.G., 1981. Convective Boiling and Condensation, second ed. McGraw-Hill.
Cumo, M., Farello, G.E., Ferrari, 1977. Heat transfer in condensing jets of steam in water (Pressure-Suppression systems). Research Report CNEN, Italy, RT/ING 8 (77).
D'Azzo, J., Houpis, C., 1988. Linear Control System Analysis and Design, Editorial Mac Graw Hill. Editorial: McGraw-Hill Inc., US, ISBN 9780070161863.
De With, A., 2009. Steam plume length diagram for direct contact condensation of steam injected into water. Int. J. Heat Fluid Flow 30, 971–982.
Finkelstein, Y., Tamir, A., 1976. Interfacial heat transfer coefficients of various vapors in direct contact condensation. Chem. Eng. J. 12, 199–209.
Fukuda, S.J., Saitoh, S., 1982. Pressure variations due to vapor condensation in liquid, (I) classification of phenomena and study on chugging, vol 24, No 6. J. Atom. Energy Soc. Jpn. 24 (No 5), 372–380.
Fukuda, S.J., 1982. Pressure variations due to vapor condensation in liquid, (II) phenomena at large vapor mass flow flux. J. Atom. Energy Soc. Jpn. 24 (No 6), 466–474.
Gallego-Marcos, I., Kudinova, P., Villanueva, W., Puustinen, M., Räsänenc, A., Kimmo Tielinenc, K., Kotroc, E., 2019. Effective momentum induced by steam condensation in the oscillatory bubble regime. Nucl. Eng. Des. 350, 259–274.
Gregu, G., Takahashi, M., Pellegrini, M., Mereu, R., 2017. Experimental study on steam chugging phenomenon in a vertical sparger. Int. J. Multiphas. Flow 88, 87–98.
Guckenheimer, J., Holmes, P., 1986. Nonlinear oscillations, dynamical systems and bifurcation of vector fields. In: Second Printing Revised and Corrected. Editorial Springer Verlag.
Gulawani, S.S., Joshi, J.B., Shah, M.S., Rama-Prasad, C.S., Shukla, D.S., 2006. CFD Analysis of Flow Pattern and Heat Transfer in Direct Contact Steam Condensation. Chem. Eng. Sci. 61, 5204–5220. https://doi.org/10.1016/j.ces.2006.03.032.
Harby, K., Chiva, S., Muñoz-Cobo, J.L., 2017. Modelling and experimental investigation of horizontal buoyant gas jet injected into stagnant uniform ambient liquid. Int. J. Multiphas. Flow 93, 33–47.
Hong, S.J., Park, G.C., Cho, S., Song, C.H., 2012. Condensation dynamics of submerged steam jet in subcooled water. Int. J. Multiphas. Flow 39, 66–77.
Komnos, A., 1981. Ein thermo-hydrodynamisches Modell zur Wiederbenetzung. Ph.D. thesis. Technical University of Munich.
Kerney, P.J., Faeth, G.M., Olson, D.M., 1972. Penetration characteristic of a submerged steam-jet. AIChe 18 (3), 548–553.
Kim, Y.S., Kung, M.K., Park, J.W., 1997. An experimental investigation of direct condensation of steam in subcooled water. J. Kor. Nucl. Soc. 29 (No 1), 45–57.
Kim, H.Y., Bae, Y.Y., Song, C.H., Park, J.K., Choi, S.M., 2001. Experimental study on stable steam condensation in a quenching tank. Int. J. Energy Res. 25 (3), 239–252.
Kryukov, A.P., Levashov, V.Y., Puzina, Y., 2013. Non-equilibrium Phenomena Near Vapor-Liquid Interfaces. Springer Briefs in Applied Science and Technology, ISBN 978-3-319-00083-1.
Lee, C.K.B., Chan, C.K., 1980. Steam chugging in pressure suppression containment. Report Nuclear Regulatory Commission NUREG/CR 1562 R4.
Li, H., Villanueva, W., Kudinov, P., 2014. Approach and development of effective models for simulation of thermal stratification and mixing induced by steam injection into a large pool of water. Sci. Technol. Nucl. Instal 2014, 11. Article ID 108782.
Linehan, J.H., Grolmes, M.A., 1970. Condensation of a high velocity vapor on a subcooled liquid jet in a stratified fluid flow. In: IHTC4 Fourth International Heat Transfer Conference. Paris-Versailles. https://doi.org/10.1615/IHTC4.1390.
Marek, R., Straub, J., 2001. Analysis of the evaporation coefficient and the condensation coefficient of water. Int. J. Heat Mass Tran. 44, 39–53.
Moody, F.J., 1990. Introduction to Unsteady Thermo-Fluid Mechanics. Editorial John Wiley and Sons, ISBN 0-471-85705-X.
Muñoz-Cobo, J.L., Verdú, G., 1991. Application of Hopf bifurcation theory and variational methods to the study of limit cycles in boiling water reactors. Ann. Nucl. Energy 18 (No 5), 269–302.
Norman, T.L., Revankar, S.T., Ishii, M., Kelly, J.M., 2006. Steam-air Mixture Condensation in a Subcooled Water Pool, Report PU/NE-06-12. University of Purdue, School of Nuclear Engineering.
Norman, T.L., Revankar, S.T., 2010-a. Jet-plume condensation of steam–air mixtures in subcooled water. Part1: Experiments. Nucl. Eng. Des. 240, 524–532.
Norman, T.L., Revankar, S.T., 2010-b. Jet-plume condensation of steam–air mixtures in subcooled water, part 2: code model. Nucl. Eng. Des. 240, 533–537.
Papanicolaou, P.N., List, E.J., 1988. Investigations of round vertical turbulent buoyant jets. J. Fluid Mech. 195, 341–391.
Petrovic, A., March 15, 2005. Analytical study of flow regimes for direct contact condensation based on parametrical investigation. ASME. J. Pressure Vessel Technol. February 127 (1), 20–25, 2005.
Plesset, M.S., 1949. The dynamics of cavitation bubbles. ASME J. Appl. Mech. 16, 228–231.
Qu, X.H., Tian, M.C., 2016. Acoustic and visual study on condensation of steam–air mixture jet plume in subcooled water. Chem. Eng. Sci. 144, 216–223.
Rodi, W., 1982. Turbulent Buoyant Jets and Plumes. The Science and Applications of Heat and Mass Transfer, Reports Reviews and Computer Programs, vol. 6. Pergamon Press, New York.
Romanelli, A., Bove, I., González, F., 2012. Air expansion in the water rocket. Am. J. Phys. 81 (10) https://doi.org/10.1119/1.4811116.
Sideman, S., Moalem-Maron, S., 1982. Direct contact condensation. Adv. Heat Tran. 15, 227–281.
Silver, R.S., Simpson, H.C., 1961. The Condensation of Superheated Steam. Proceedings of a conference held at the National Engineering Laboratory, Glasgow, Scotland.
Simpson, M.E., Chan, C.K., 1982. Hydrodynamics of a subsonic vapor jet in subcooled liquid. J. Heat Tran. 104 (2), 271–278.
Song, C.H., Kim, Y.S., 2011. Direct contact condensation of steam jet in a pool. Adv. Heat Tran. 43, 227–283.
Schrage, R.W., 1953. A Theoretical Study of Interphase Mass Transfer. Columbia University Press, New York.

Soh, W.K., Karimi, A.A., 1996. On the calculation of the heat transfer in a pulsating bubble. Appl. Math. Model. 20 (September), 638–645, 1996.
Sun, J., Ran, X., Zhang, Z.X., Fan, G., Ding, M., 2020. Effects of direct contact condensation on flow characteristics of natural circulation system at low pressure. Front. Energy Res. 8, 173.
Urban, C., Schlüter, M., 2014. Investigations on the stochastic nature of condensation induced water hammer. Int. J. Multiphas. Flow 67, 1–9.
Van Reeuwijk, M., Salizzoni, P., Hunt, G., Craske, J., 2016. Turbulent transport and entrainment in jets and plumes: a DNS study. Phys. Rev. Fluids 1, 074301.
Villanueva, W., Lia, H., Pustinen, M., Kudinova, P., 2015. Generalization of experimental data on amplitude and frequency of oscillations induced by steam injection into a subcooled pool. Nucl. Eng. Des. 295, 155–161.
Wang, J., Chen, L., Cai, Q., Hu, C., Wang, C., 2021. Direct contact condensation of steam jet in subcooled water: a review. Nucl. Eng. Des. 377, 111142.
Wu, X.Z., Yan, J.J., Shao, S.F., Cao, Y., Liu, J.P., 2007. Experimental study on the condensation of supersonic steam jet submerged in quiescent subcooled water: steam plume shape and heat transfer. Int. J. Multiphas. Flow 33 (12), 1296–1307.
Zhao, Q., Cong, Y., Wang, Y., Chen, W., Chong, D., Yan, J., 2016. Effect of non-condensation gas on pressure oscillation of submerged steam jet condensation. Nucl. Eng. Des. 305, pp110–120.
Zhao, Q., Chong, D., Chen, W., Li, G., Yan, J., 2020. Review: steam cavity characteristics of steam submersed jet condensation at SC regime. Prog. Nucl. Energy 130 (2020), 103560.

Nomenclature

Latin symbols

A_i: Interfacial area (m^2)
$A(x)$: Jet transverse area at a distance x (m^2)
B: Condensation driving potential
c_p: Specific heat at constant pressure ($\frac{J}{kg°K}$)
$d_1(x)$: Jet diameter in the steam dominated region
$d_2(x)$: Jet diameter in the liquid dominated region
$d_v = 2r_0$: Vent diameter (m)
$\widehat{f}_c$: Accommodation factor for condensation
$\widehat{f}_e$: Accommodation factor for evaporation
f_{oscill}: Oscillation frequency of the steam jet (s^{-1})
G: Mass flux (kg/m^2s)
h: Heat transfer coefficient ($J/m^2s°K$)
h_{fg}: Specific enthalpy of phase change (J/kg)
Ja: Jakob number
l_p: Jet penetration length (m)
l_s: Average jet penetration length during the oscillations (m)
M: Molecular weight of the steam
m''_c: Condensing mass flux at the interface (kg/m^2s)
n: Polytropic exponent
Nu: Nusselt number
p_s: steam pressure
q''_i: Interfacial heat flux (J/m^2s)
Q: Volumetric flow rate (m^3/s)
$r(x)$: Jet radius (m)
r_0: Radius of the vent at the exit
R: Universal gas constant
S_m: Transport modulus (Stanton number)
T: Temperature (°K)
u_e: Entrainment velocity (m/s)
u_l: Liquid velocity (m/s)
V_0: Header volume (m^3)
V_s: Steam volume (m^3)
W_s: Steam mass flow rate (kg/s)
X: Distance from the vent exit to the beginning of the liquid dominated region (m)
$X_p = \frac{l_p}{r_0} = \frac{2l_p}{D_0}$: Nondimensionalized jet penetration length

Greek symbols

α: Expansion angle in the steam dominated region
α_E: Entrainment coefficient
β: Jet expansion angle in the liquid dominated region
ε: Order parameter in perturbation theory
λ_i: Lyapunov exponents (s^{-1})
ν: Coefficient that gives the variation of the volume with the characteristic length
ρ: Density (kg/m^3)